Experimental Tools for Studies of Heterogeneous Catalysis

-

Development and Case Studies

Jonas Evertsson

Diploma work 60 ECTS credits 2013

Supervisor: **Johan Gustafson**

Division of Synchrotron Radiation Research

Physics Department

LUND UNIVERSITY

1 Content

2 Populärvetenskaplig sammanfattning

Jonas Evertsson

Utveckling och testning av reaktorer för katalysmätningar

Katalysatorer är oumbärliga i såväl livsprocesser som industriella tillämpningar. Bilismen är ett exempel där katalysatorer används vid såväl bränsletillverkning som avgasrening. Men detta är långt ifrån det enda användningsområdet. Katalysatorer är också delaktiga i tillverkningen av uppemot 90% av alla kemikalier.

Industriella katalysatorer för oxidering av kolmonoxid och metan, CO och CH_4, är mycket komplexa system som ofta består av katalytiskt aktiva nanopartiklar utspridda i ett supportmaterial. Sådana katalysatorer är svåra att undersöka med ytfysikens metoder. Därför har det under många år använts modeller med enkla kristallprover, ultrahögvakuum och ex situ metoder, tillvägagångssätt som långt ifrån avspeglar industriella katalysatorer. Under senare år har nya in situ tekniker utvecklats och därmed möjligheter till att studera mer realistiska modeller som i sin tur bidrar till ökad förståelse.

I mitt examensarbete har jag bidragit till detta genom att testa och utveckla fyra typer av reaktorkammare där masspektrometri, lasertekniken PLIF och röntgendiffraktion har använts för att karakterisera flera typer av katalytiska system, från enklare modeller till mer verkliga som används av industrin.

Med den första reaktorn var det möjligt att göra aktivitetsmätningar av katalysatorer med masspektrometri för temperaturer upp till minst 1000°C. Med reaktorn gjordes flera aktivitetsmätningar av metan oxidering över olika palladiumfolier, vilket visade på flera intressanta resultat.

Med den andra reaktorn användes PLIF för att göra aktivitetsmätningar av tre katalysatorer samtidigt. Detta testades för CO oxidation och resultatet var lovande. Men mindre ändringar behövs för att kunna göra metan oxidation.

Den tredje och fjärde reaktorn möjliggjorde kombinerad masspektrometri och röntgendiffraktionsmätningar av både gasen och den atomära strukturen hos katalysatorerna. Mätningen med den fjärde reaktorn var lovande och det var möjligt att följa strukturförändringar samtidigt som det pågår reaktioner på katalysatorerna. Men också här skulle det behövas en mindre förändring för att kunna följa processen tydligare.

Eftersom många delar av världen är på väg att industrialiseras behövs troligtvis bättre, billigare men också nya katalysatorer till reaktioner där katalysatorer tidigare inte använts. För att utveckla dessa måste troligtvis kunskapen om katalys på grundläggande atomär nivå öka, vilket i sin tur betyder att också nya metoder behövs.

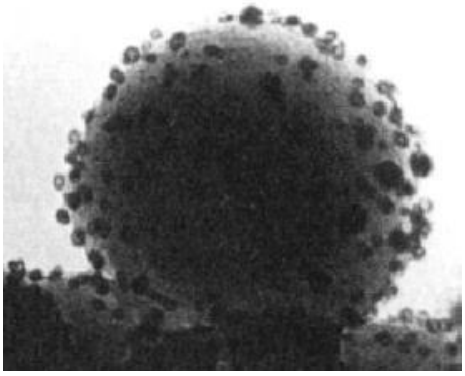

Katalytisk nanopartikel. Bild från A.K. Datye, N.J. Long, *Ultramicroscopy* 25, (1988), 203

Handledare: **Johan Gustafson**
Examensarbete 60 hp i fysik 2013
Fysiska institutionen, Lunds universitet

*Examensarbetsämne: se kursplan

3 Abstract

In this project four reactors for studies of heterogeneous catalysis have been developed. They were tested using case studies, especially concerning methane oxidation over palladium. The test measurements showed that the reactors work or would work very well after slight modifications.

The first reactor allowed for activity measurement using mass spectrometry for temperatures up to at least 1000°C. The reactor was tested with methane oxidation over different palladium foil samples.

With the second reactor it is possible to perform activity measurements of three catalysts simultaneously using planar laser induced fluorescence. The reactor was tested with CO oxidation over three different monolith catalysts. From the measurement it was possible to follow the activation process of the three catalysts simultaneously. However, it was not possible to study methane oxidation due to the higher temperature needed to run this reaction, but with minor modifications, this should be possible as well.

The third and fourth reactor allowed for structural studies of powder catalysts using X-ray diffraction. It was tested using methane oxidation over Pd/Al_2O_3 powder catalyst. The result showed that it is possible to see when the palladium particles are metallic and when they are oxidized. But also here a slight modification is needed before really good result can be achieved.

The different case studies also reveal some interesting results, which are discussed further in the report and would be interesting to study further in the future.

4 Introduction

In 1836, catalysis was defined by Berzelius as a process, where a reaction is accelerated by another substance, a catalyst, which itself is not consumed [1]. A well-known example of the application of catalysis is for automotive exhaust cleaning, where a catalyst is used to clean the exhaust from the toxic gases, such as carbon monoxide (CO) and nitrogen oxides (NO_x). But this is far from the only important application. Catalysts are today involved in the manufacturing of up to 90 % of the products in the chemical industry [2].

In this project heterogeneous catalysis was studied, where the reactants are gases and the catalysts are metals. In industry a heterogeneous catalyst is usually very complex, consisting of small nanoparticles, and used at high pressures. These systems are very difficult, if not impossible, to study in a basic atomic level. Hence these catalysts have been developed using a trial-and-error approach, without proper knowledge about how they work on the atomic level.

Over the last decades however, catalytic processes have been studied in the field of surface science using simplified model systems and the level of understanding has increased. In 2007 Gerhard Ertl was awarded a Nobel Prize for his studies of the catalytic processes over model surfaces [3].

The model systems traditionally studied in surface science are single crystals in ultra-high vacuum (UHV), which allows for maximum control of the molecules and atoms at the surface. These conditions are far away from the realistic systems used in the industry, and the question is if the knowledge from such simple systems is applicable to realistic systems. The difference between the models and realistic systems is usually referred to as the pressure gap and the materials gap. Later, due to technical advances it has been possible to study more complex systems on a more basic level and the gaps have started to shrink.

The aim of the research is of course to improve the catalysts, but also to find materials cheaper than the expensive metals, for example the transition metals, that are used today as catalysts for many reactions.

In this project I have contributed to this by developing and testing four different reactors that allow for *in situ* studies of more complex or even actual realistic systems at high temperatures. The reactors were tested with methane (CH_4) oxidation over different palladium (Pd) and platinum (Pt) catalysts. In methane oxidation, CH_4 is oxidized to carbon dioxide (CO_2) and water (H_2O), according to the complete reaction path, or to CO and hydrogen (H_2), according to the partial reaction path. Since CH_4 is rather inert and a higher temperature is needed to run the reaction, CO oxidation, which runs at lower temperature, was also used to test one reactor. In CO oxidation, CO is oxidized to CO_2.

CH_4 is interesting to study in many aspects. It is for example the main component of natural gas, which is used as a fuel and since it is a potent greenhouse gas, catalysts are needed for cleaning of the unburned fuel [4].

Through partial oxidation of CH_4 a mixture of CO and H_2 is produced, which is referred to as syngas and in turn can be converted to different liquid hydrocarbons through the collection of reactions included in the so called Fischer-Tropsch process [5]. As the partial oxidation path competes with the more favored complete oxidation path of CH_4, it is of interest to understand and develop catalysts that are more selective for the partial oxidation path.

The first reactor developed allows for activity measurement using mass spectrometry (MS) for temperature up to at least 1000°C. This reactor was tested using case studies of CH_4 oxidation over Pd foils and yielded several interesting results.

The second reactor, allowed for activity measurement using planar laser induced fluorescence (PLIF) of three catalysts simultaneously. This was tested with CO oxidation and the results are promising. However, slight modifications are needed to allow for studies of CH_4 oxidation.

With the third and the fourth reactor, it was possible to follow structural changes of the catalysts using X-ray diffraction (XRD). The fourth reactor is very promising. Also here a slight modification would allow for extensive studies of the catalyst structure during catalytic processes up to high temperatures.

5 Catalysis

Catalysis can be divided into homogenous, when the catalyst and reactants are in the same phase or heterogeneous, when they are in different phases. This project covers heterogeneous catalysis, in which the reactants are in gas phase and catalysts are solids. Several reactions and catalysts are investigated in this project but the main focus is on CH_4 oxidation over different Pd catalysts.

As said, the catalyst accelerates a reaction that most often can happen uncatalyzed by providing an alternative reaction path. Figure 5.1 illustrates both the uncatalyzed (dashed) and the catalyzed (solid) paths for a reaction over a metallic catalyst. The uncatalyzed path includes an intermediate state with very high energy and is therefore slow. The catalyzed path is energetically much more favourable, but also includes more steps that complicate the reaction process. For example, the reactants must be able to adsorb on the catalyst, but not too strongly since they still must be able to react and finally desorb from the surface as products. In addition, in many catalytic reactions, including CH_4 and CO oxidation, one or more reactants must dissociate. Gas phase dissociation is a very energy consuming process and often the reason for the high energy barrier in the uncatalyzed path. Over a catalyst, however, this process is much more favourable and therefore faster.

This chapter first more generally introduces the different steps of heterogeneous catalysis, where the more studied CO oxidation is used as an example, and secondly describes the case of CH_4 oxidation over Pd more extensively. The basics about catalysis are covered in references as [2] and [6].

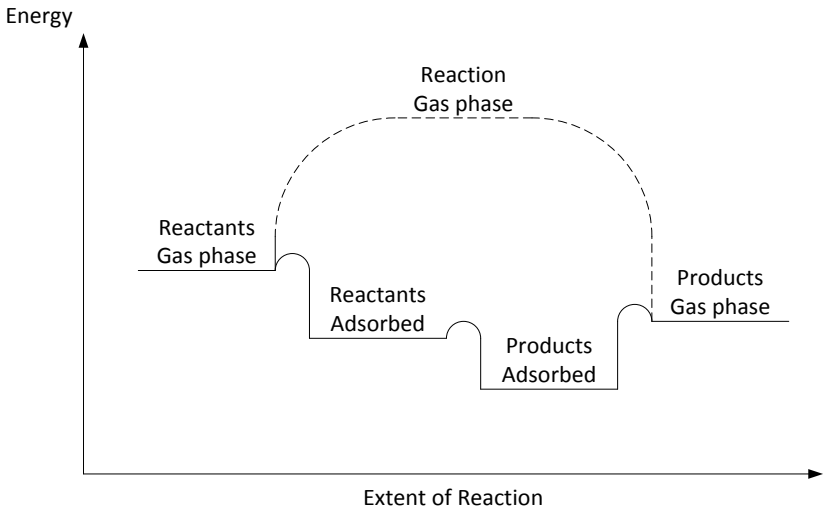

Figure 5.1. Energy diagram of a reaction that is catalyzed (solid) and uncatalyzed (dashed).

5.1 Electronic structure of molecules

In the catalyzed reaction molecules (reactants and products) should interact with a surface and also each other. Due to the difference between molecules, the results from the interaction with the surface can be different. For example, some of the reactants are dissociated as they are adsorbed at a surface, but others are adsorbed without dissociating. Below the difference between the molecules electronic structure is introduced or in another word, their orbital structure. This is later used to explain the difference in their interaction with the catalyst.

The orbitals of a molecule can be divided into some bonding and some anti-bonding orbitals that, if compared to the atomic orbitals, have lower and higher energy, respectively [7]. Figure 5.2 illustrates this for two naturally occurring molecules, O_2 and CO. The 2s and 2p atomic orbitals are split into some bonding orbitals σ, π and some anti-bonding orbitals σ^*, π^* in the molecule.

It is energetically favourable for atoms to form a molecule when more of the molecular bonding orbitals are filled with electrons than the anti-bonding orbitals. Since the orbitals are filled in increasing energy order, the number of electrons, for natural occurring molecules, is so many such that this is fulfilled. The bond strength of a molecule depends on the number of electrons that fill the bonding and the anti-bonding orbitals, respectively. More electrons in the bonding orbitals give a stronger bond and more electrons in the anti-bonding orbitals give a weaker bond.

If comparing O_2 and CO, both of them are energetically favourable to be formed, since more electrons (blue balls) fill the bonding than the anti-bonding orbitals, but the bond strength of O_2 is weaker as there are two more electrons in the anti-bonding orbital π^* of O_2.

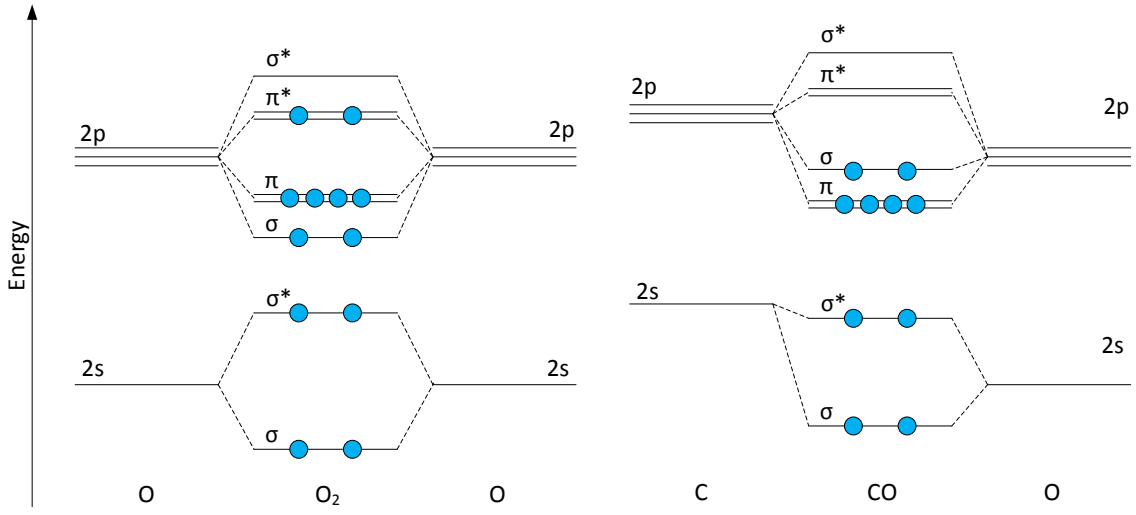

Figure 5.2. Molecular orbital diagram of O_2 and CO. The blue balls indicate the electrons that fill the molecular orbitals. The figure does not show the four electrons that fill the lowest molecular orbitals from the splitting of the 1s states in the atoms.

5.2 Interaction between surfaces and molecules

The interaction of the surface with the reactants and products is of course important for the catalytic reaction as the surface is where the reaction takes place. Here are the concepts of adsorption introduced and how this makes it possible for the reactants to adsorb, react and desorb as products.

5.2.1 Adsorption

The first step in the catalytic cycle is for the reactants to adsorb at the surface. Figure 5.3 shows a simplified energy diagram of the different adsorption states for a di-atomic molecule approaching a surface. The molecule can either more directly go into one of the adsorption states or go back and forth between them. There exist two different types of adsorptions, the weaker physisorption and the stronger chemisorption. A molecule can chemisorb without dissociating (associate chemisorption) or dissociate as it is chemisorbed (dissociative chemisorption). The dissociative chemisorption is important for some catalytic reactions, for example CO oxidation and CH_4 oxidation. The different adsorption processes are introduced below.

5.2.1.1 Physisorption

Physisorption is the weaker kind of adsorption, but also the most long ranging and easiest to induce. The force is due to van der Waals interaction between the adsorbate (molecule or atom) and adsorbent (surface). The van der Waals interaction is the force between two dipoles induced by the adsorbate and adsorbent itself. The intensity of the interaction depends on how easily the electrons of the adsorbate and adsorbent can be redistributed.

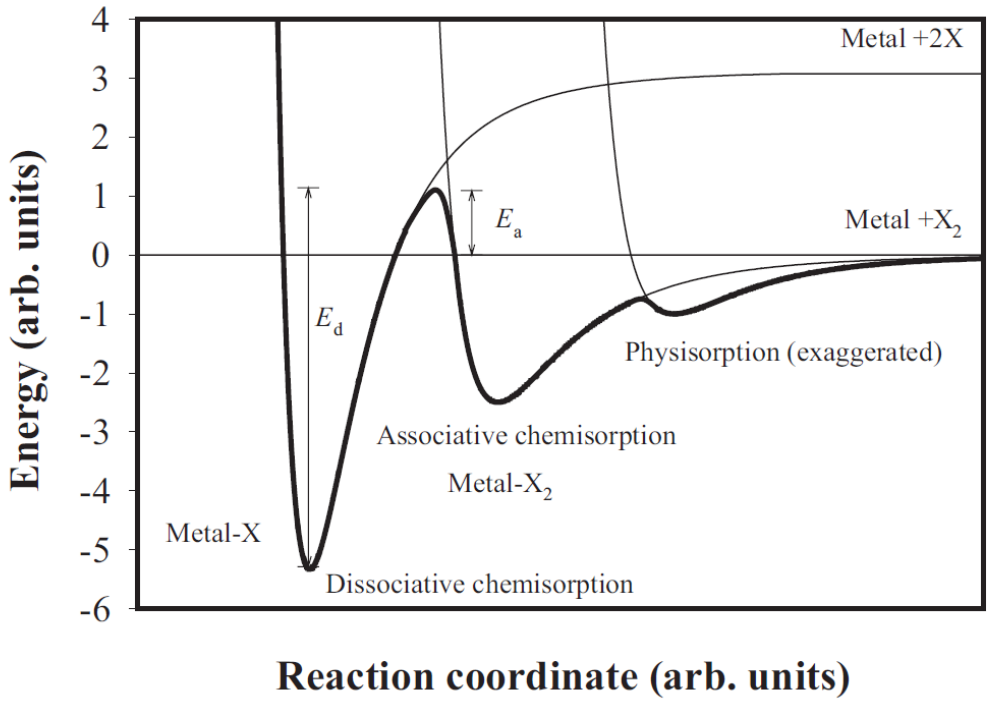

Figure 5.3. A simplified energy diagram showing the different adsorption states for a di-atomic molecule (X_2) that approaches a catalytic metal surface. [2]

5.2.1.2 Chemisorption

Chemisorption is stronger, but not as long ranging and is more difficult to induce. The force between the adsorbate and adsorbent is called a chemical bond and is similar to the force between atoms in molecules. Characteristic for the chemical bond is that electrons are shared in metallic, ionic or covalent bonds.

5.2.1.3 Adsorption on d-band transition metals

Transition metals, which usually are good catalysts, have a sp-band, as all metals, but also a d-band. The interaction between this d-band with the molecular orbitals is important. When the molecule interacts with the catalytic surface, electrons from the metallic d-band are shared to the free orbitals of the molecule and a bond is formed between the molecule and the surface. If mostly anti-bonding orbitals of the molecule are filled, the molecular bond strength decreases and dissociation may occur.

For the example of O_2 and CO in figure 5.2, four more electrons are needed in O_2 to fill the anti-bonding orbitals to the same extent as the bonding orbitals, but for CO, six electrons are needed. Hence, the O_2 easier dissociates at the surface than CO or actually, over transitions metals during correct conditions, O_2 almost always dissociates, but CO does not.

5.2.2 Desorption

The last step of the catalytic cycle is the desorption process. Both the reactants and the products can desorb from the surface, but in many cases, including the ones considered in this project, the products are more stable on their own and weaker bound to the surface than the reactants. Therefore, at right conditions, it is possible for the products but not the reactants to desorb.

5.2.3 Formation of structures

At lower pressures, the number of adsorbates on the surface is low and they can move over the surface more freely, only interacting with the surface and stick to different more energetically favourable sites at the periodic surface. At higher pressures, however, the number of adsorbates is increased. The number of adsorbates and the lateral interaction between them makes it less probable for them to lower their energy individually at these sites as they already are occupied. Instead they can form different energetically favourable structures by mixing with the metal and, in the case of oxygen adsorption, form oxides. Since a realistic catalyst operates in higher pressures, the effect of these structures is of major importance.

Much work in this project has been to see how different oxygen structures change the activity of a catalyst. Figure 5.4 shows an example of different structures that can be formed over a Rhodium crystal at different temperatures, CO and O_2 partial pressures: (a) shows an inactive CO poisoned surface, since CO covers the surface and blocks the oxygen from adsorbing. (b) shows an inactive surface completely covered by an oxide, which blocks the CO from adsorbing. (c) shows an active surface partly covered by an oxide, which still allows CO to adsorb at the metal. (d) shows an active oxygen covered surface, as it still allows CO to adsorb. This example shows that besides the metal, also other structures can be catalytically active.

For long, it has been a debate if the oxides are active phases for realistic catalysts operating at higher pressures. Lately, technical improvement has made it possible to study catalyst in

more realistic conditions and it has been seen that there can be oxides present when the catalyst is active [8, 9, 10, 11].

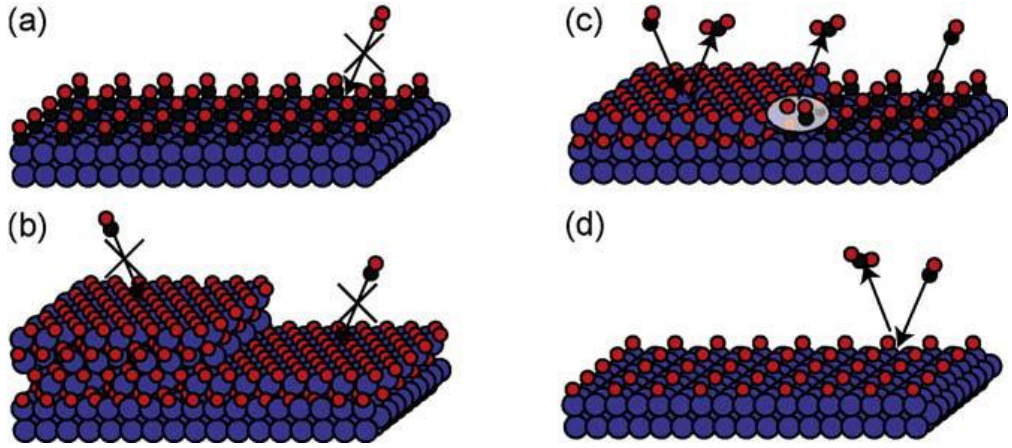

Figure 5.4. Different active structures at an Rh surface formed at different temperatures and carbon monoxide and oxygen partial pressures. (a) shows an inactive surface due to CO poisoning, which is a CO covered surface that blocks oxygen from adsorbing. (b) shows an inactive surface due to an oxide that blocks CO from adsorbing. (c) and (d) shows two active surfaces since both CO and oxygen can adsorb. [8]

5.3 Reaction rate

During the measurements in this project, the activity or the reaction rate was measured at different temperatures. It can therefore be interesting to know how the activity depends on the temperature. A simple, but often very good approximation is given by the Arrhenius equation

$$k(T) \propto e^{-E_a/k_bT}$$

where $k(T)$ is the reaction rate, E_a is the activation energy for the reaction to happen, k_b the Boltzmann constant and T the temperature, which shows that the activity increases exponentially with the temperature. This relationship is also the reason why the activity sometimes is plotted with a logarithmic scale against the inverse temperature, a so called Arrhenius plot. The slope of such plot yields the activation energy of the reaction, as seen in

$$\ln\big(k(T)\big) \propto -\frac{E_a}{k_bT}$$

Plotting like this can be good if different surface reconstructions should be recognized, as they have different activation energies. This equation does not take into account everything. For example, when the temperature is high enough, the activity flattens out, since it is instead of the temperature limited by how fast reactants can reach the surface. This is called the mass transfer limit (MTL).

5.4 The Model catalysts

The realistic industrial catalysts usually consist of smaller particles of transition metals sitting on a support. The main purpose for the support is to prevent the active particles from sintering into larger. Smaller particles of the expensive metals are desired, since for the same amount of material, smaller particles have a larger total surface area than larger particles.

But these small particles are difficult to study in detail. Hence, the industry has for many years developed the catalyst in a trial and error method. Detailed knowledge of catalysis has instead emerged from surface scientific studies of very simple model system, where single crystals and ultra-high vacuum are used. The question is if the knowledge from these models is relevant also for realistic catalysts. This gap between the realistic industrial and the model catalysts is in the surface science community referred as the materials and pressure gap.

Lately, however, new technical advances have made it possible to investigate more realistic model catalysts in more realistic conditions, which consequently have increased the level of understanding.

In this project, metallic foils, powders and monolith catalyst were studied. These models included the for CH_4 oxidation active metal Pd or Pt. The models can be seen as something between the very surface technique friendly single crystal and the realistic industrial catalyst. The models are further described below.

5.4.1 Foil samples

The properties of these samples are not studied with surface sensitive techniques and therefore not qualitatively known. Anyway, probably the surface is between that of a crystal and that of a particle of the same material. The samples can in that way be seen as a bridge between the more surface technique friendly crystal and the more industrial like powder. Also a palladium-silver alloy (PdAg) is investigated to see how the silver (Ag) affects the activity. Ag is cheaper than Pd and could be used to produce less expensive catalysts.

5.4.2 Supported samples

As mentioned, the supports should prevent the small metallic particles from sintering. But at the same time, the support influences the catalytic process by interacting with the metal particles and the gas. These interactions can both increase or decrease the performance of the catalytic process.

In this project, the supports Alumina (Al_2O_3) and Ceria (CeO_2) were studied. A supported catalyst is often denoted as #% metals/support. For example, 2%Pt/Al_2O_3 is an alumina supported catalyst with 2% (weight percent) platinum. The supported models were in shape of powders or monoliths. Figure 5.5 (a) is an image of a supported catalyst particle, where the expensive metals is supported on porous structure.

Figure 5.5 (b) shows a photo of monolith. The monolith is a multichannel ceramic structure that mostly consists of cordierite. It is impregnated by dipping it in solutions including the support material and the metal, sometimes several times. After the impregnation the monolith is calcined in higher temperature (~500℃). It is possible by doing the steps in different ways to get different desired properties of the final monolith catalyst.

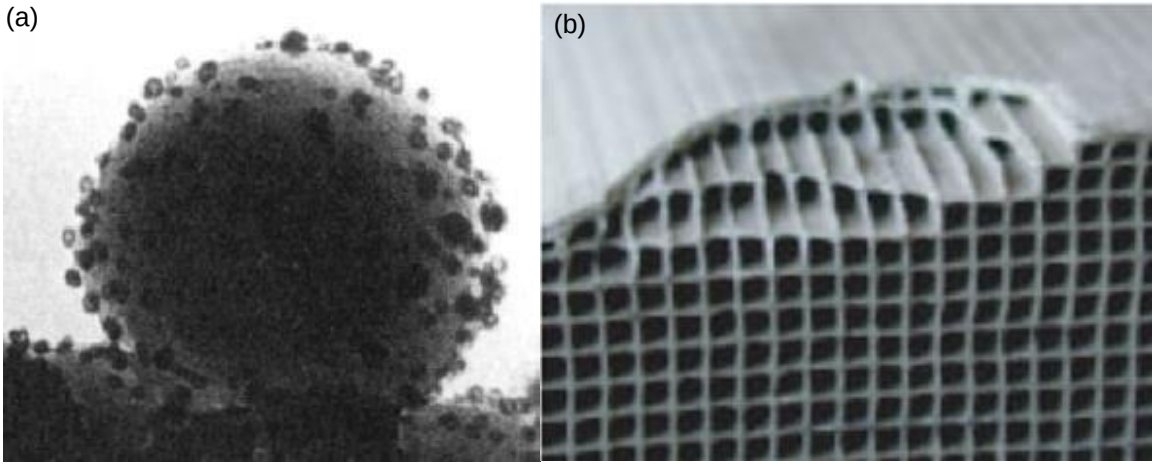

Figure 5.5. (a) is an image of a supported catalytic nanoparticle [12]. (b) is a photo of a monolith. [2]

5.5 Case of methane oxidation over Pd

In this project, the complete

$$CH_4 + O_2 \rightarrow CO_2 + 2H_2O$$

and partial

$$2CH_4 + O_2 \rightarrow 2CO + 4H_2$$

oxidation of CH_4 over different catalysts, including Pd and Pt, were studied. Both of them happen simultaneously, but the complete oxidation is overall more favourable. However, by the relative concentration of reactants it is possible to promote each of them. In an excess of O_2, the complete oxidation is promoted and in an excess of CH_4 the partial oxidation is instead promoted.

Included in the process is the dissociation of both O_2 and CH_4. O_2 dissociates at the surface without, or almost without, an energy barrier, but for CH_4 it includes a significant high energy barrier. Actually, the dissociation of CH_4 is so slow that this is the rate determining step (RDS) of the reaction [13].

The temperature dependence on the kinetics for CH_4 oxidation over Pd catalysts has shown to be peculiar. Figure 5.6 shows the result from a combined mass spectrometry (MS) (a) and surface X-ray diffraction (SXRD) (b) CH_4 oxidation measurement over a Pd(100) crystal surface during a temperature ramp [11]. CH_4 and O_2 were flown over the catalyst and the condition before any reaction was 6 mbar CH_4 and 16 mbar O_2. In order to increase the sensitivity, the flow was stopped for short times during the measurement, such that the CO_2 pressure was built up. This is seen as the smaller peaks in the CO_2 signal.

As the temperature is ramped up, the activity peaks at two temperatures, at 500°C and 590°C and again when the temperature is ramped down. The SXRD plot shows the intensity at a reflection from an oxide. The oxide is present when the lower temperature active phase occurs, but as the oxide gets thicker (SXRD intensity increases) the activity decreases. The activity goes up again first when the oxide has desorbed (SXRD drops significantly) and the surface is metallic.

Together with theoretically calculations (density functional theory) of the dissociation barrier for CH_4 on different possible dissociation sites, the phases could be deduced. The low temperature active phase was deduced to be sites on a PdO(101) structure that was exposed when the oxide was thinner and the higher active phase at 590°C due to sites in the metal. In between the two active phases, however, there is an inactive oxide. This was deduced to be sites at a PdO(100) surface, which is exposed when the oxide is thicker and has a significantly higher energy barrier for methane dissociation. The experiment shows that both the metallic and oxidized Pd can be active structures for CH_4 oxidation, but it has to be the right oxide structure. In addition it was shown that the ultra-thin surface oxide (a single layer of PdO(101)) was inactive. Similar temperature dependence of the activity has also been reported for Pd foils [14] and other single crystals [15].

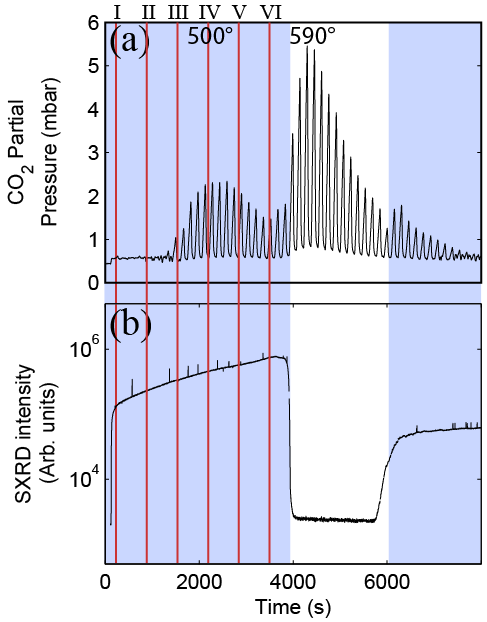

Figure 5.6. Result from a combined MS (a) and SXRD (b) measurement of methane oxidation over a Pd(100) crystal during a temperature ramp. The temperature is ramped up and down and peaks at 590°C. The SXRD measures the intensity from a reflection from of an oxide. The activity peaks at both 500°C and 590°C in the up ramp. The measurement shows that both a proper oxide and the metal are active for methane dissociation and consequently methane oxidation. [11]

6 Experimental methods

The aim of the project was to study how the activity over the catalyst depends on the interaction between gases and surfaces. To do this, three methods were used; mass spectrometry (MS), X-ray diffraction (XRD) and planar laser induced fluorescence (PLIF). MS and PLIF provide information of the gas composition. XRD, on other hand, yields information of the crystal structures of the catalyst. This chapter describes the different methods and how they are applied for studies of catalytic processes.

6.1 Diffraction

With different diffraction methods it is possible to measure the periodicity of different systems. In this project X-rays were used to study the crystal structures of powdered catalysts. This is usually referred to as powder diffraction. Below, the crystal structure of solids and the theory of X-ray diffraction are introduced. Later, the powder diffraction method is more explicitly described. The basic theory of crystal structures and X-ray diffraction is covered in reference [16] and the powder diffraction method more explicitly in reference [17].

6.1.1 Crystal structure

The atoms in a solid are usually ordered in a periodic lattice crystal. The lattice is defined by its base vectors such that the distance between two arbitrary points in the lattice is a linear combination of the vectors. Figure 6.1 (a) shows the simplest case of a 2 dimensional periodic lattice, which is defined by the base vectors **a** and **b**. Each lattice point consists of an atom or in more complicated structures, a group of atoms. The group is called a basis and is in (a) only one atom, but in the more complicated structure in (b) two atoms (dashed ellipsoid). The volume defined by the base vectors is a so called unit cell (grey in the figure). Around each lattice point the environment in the volume of the unit cell is identical. The whole lattice structure can therefore be seen as build-up of many stacked unit cells.

In most cases it is possible to describe the lattice with different sets of base vectors and basis. Figure 6.1 (c) illustrates a lattice that is described by two sets of base vectors that have one or two atoms in the basis, respectively. Due to practicality the lattice is usually described using base vectors with right angles between them.

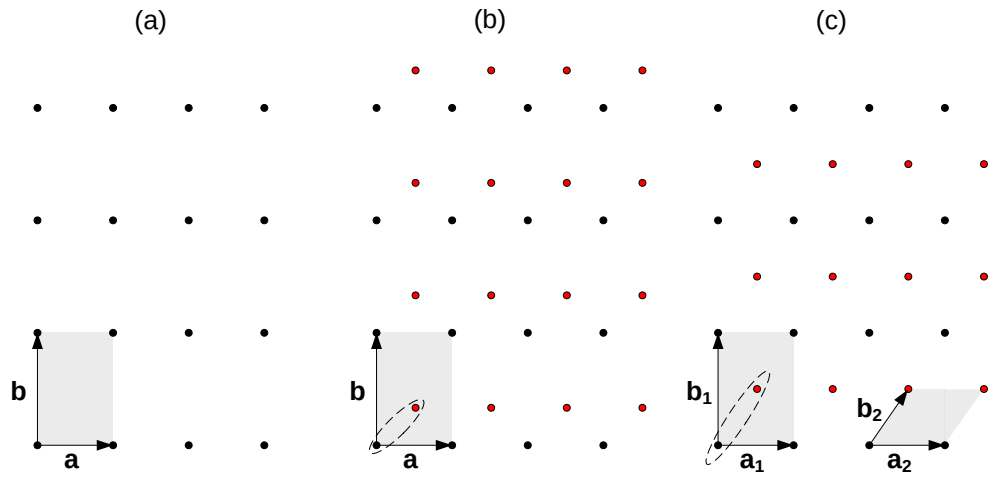

Figure 6.1. Illustration of different two dimensional lattices. (a) is a lattice with one atom in the basis. (b) is a lattice with two atoms in the basis. (c) is a lattice with one or two atoms in the basis depending on the base vectors.

For metals the atomic structure is usually described by cubic 3 dimensional lattices, which base vectors have the same length. Figure 6.2 show three examples of unit cells for different lattices; (a) the simple cubic (sc), (b) body-centered cubic (bcc) and (c) face-centered cubic (fcc), where they have 1, 2 and 4 atoms in the basis, respectively. (c) shows also an alternative definition of the base vectors, where only one atom is needed in the basis. The metals Pd and Pt, which are studied in this project, have the cubic fcc lattice structure.

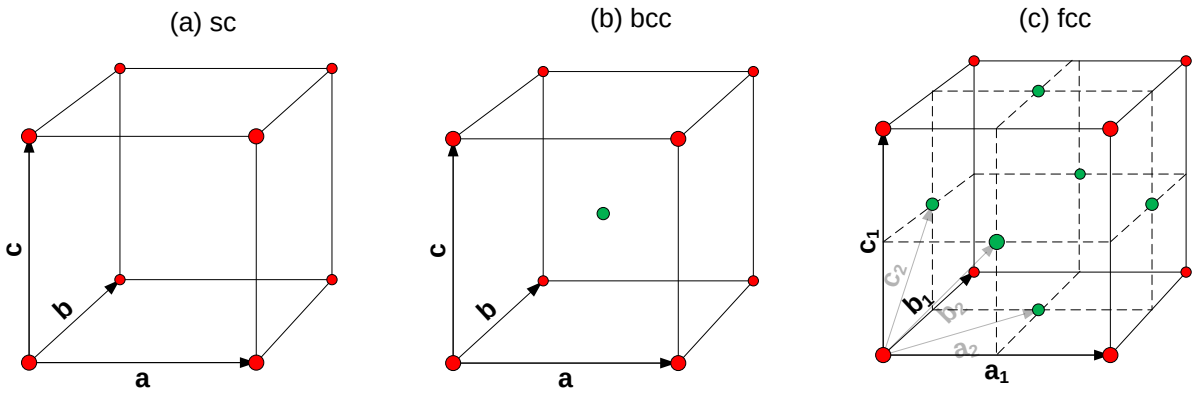

Figure 6.2. Three examples of unit cells for different 3 dimensional lattices. (a) the simple cubic (sc), (b) body-centered cubic (bcc) and (c) face-centered cubic (fcc).

Each crystal has a structure that is specific for that crystal. It can be different unit cells of at least different lattice constants. The lattice constant is the distance between the unit cells in the crystal. This individuality can be used to distinguish between different crystalline solids.

The structures that can be formed on a catalyst, for example oxides, are also crystalline with a specific structure. These structures are usually more complicated and are therefore not described here.

6.1.2 Crystal planes

As a consequence of the periodic crystal structure, the atoms can be seen as positioned in different parallel planes, as illustrated in figure 6.3 for three examples (blue, green and black). The distance between adjacent planes of the same orientation is the same for all planes that have this orientation. Since each crystal is specific also these adjacent distances is specific for each crystal.

The orientation of a plane is usually described by the so-called Miller indices (hkl). The numbers h, k and l are the inverse of the interception between the plane and the x, y and z axes that are parallel to the base vectors **a**, **b** and **c**, respectively. Since the axes x,y and z can be described by a multiple of the baser vectors **a**, **b** and **c**, respectively, the interception coordinates between the plane and axes can be written as (**a**/h, **b**/k, **c**/l) or a multiple thereof.

As the interception coordinates depend on in which lattice point the axes starts, the Miller indices for a plane are defined such that each index is an integer and as close to zero as possible. This means that each set of parallel planes will be given the same Miller indices.

Figure 6.4 shows three examples of possible planes in an fcc lattice. The middle plane intercepts the x and y axes after one lattice constant a and never with the z axes, which

gives the interceptions coordinates $(x, y, z) = (a, a, \infty)$. Hence the miller indices for this plane, which is the inverse and the nearest integers, is then $(x, y, z) = a\left(\frac{1}{a}, \frac{1}{a}, \frac{1}{\infty}\right) = (1,1,0)$.

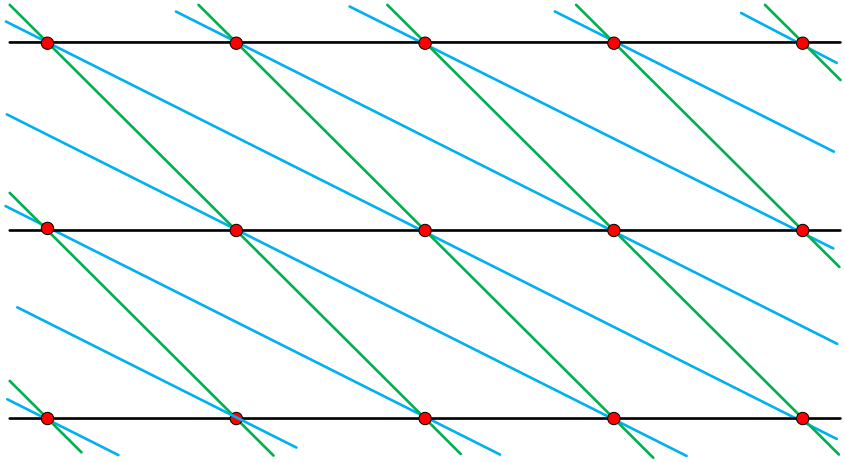

Figure 6.3. Three examples (blue, green and black) where the atoms can be seen as positioned in different parallel planes.

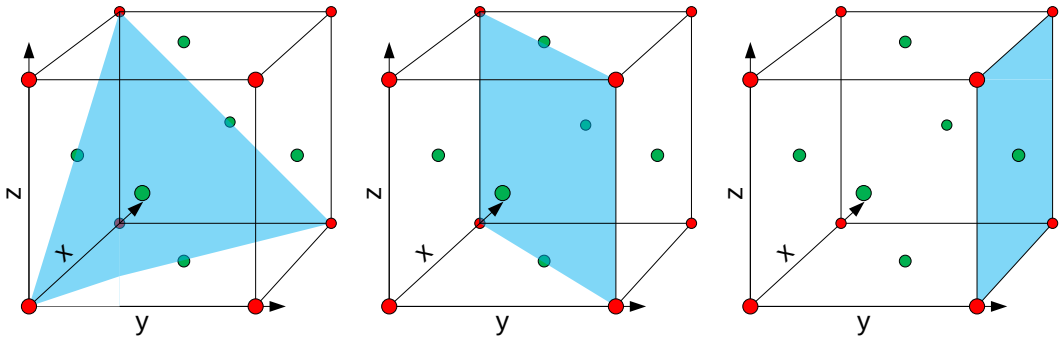

fcc(111) fcc(110) fcc(010)

Figure 6.4. Three examples of planes in an fcc lattice defined using the miller indices.

6.1.3 X-ray Diffraction

A way to measure the crystal structures is by X-ray diffraction. If the wavelength of the radiation is in the optical range, around 5000 Å, the beam is optically reflected at the crystal surface, but if the wavelength is in the same order or lower than the lattice constant, ~Å for atomic crystals, diffracted beams can be found at angles far from the ordinary optical reflections. This makes hard X-rays, <1 Å, well suited for bulk crystal studies, as it also has a long mean free path, i.e. it can reach far into the bulk of crystals. Since the catalytic reaction takes place at the surface, it would be desirable to use a more surface sensitive method. Such methods do, however, not work for powder samples in pressures up to 1 atmosphere. Hence we investigate the relation between bulk structure and catalytic activity, and assume that any structural change in the bulk will also affect the surface.

An explanation of the diffraction from crystals was given by W. L. Bragg in what is called Bragg's Law. Assume that a beam of X-rays is incident on the periodic planes of a crystal with an angle θ, where the distance between two adjacent planes are d, as seen in figure 6.5. At every plane a small fraction of the beam is reflected and when they meet again they will interfere. The interference will be constructively if they are in phase or destructively if

they are out of phase. For the X-rays to be in phase the phase difference between them should be a multiple of the wavelength. The phase difference will in turn depend on the path difference between the reflections from different planes. The path difference is the difference between two possible paths for coherent radiation. In this case the path difference between reflections from adjacent planes is equal to $2dsin(\theta)$, as seen in figure 6.5. For most of the cases, the reflected X-rays will interfere destructively resulting in no or minor diffracted beams. But if the path difference between reflections from adjacent planes is equal to a multiple n of the x-ray wavelength λ, i.e.

$$2d\sin\theta = n\lambda, \quad (6.1)$$

the reflected X-rays from all planes is in phase and will interfere constructively into a highly intense diffracted beam. Equation 6.1 is the Bragg's Law and the angles for which the law is fulfilled are called Bragg angles. The law is a consequence of the periodic structure of crystals. The X-rays are actually scattered in all direction by the atoms in the crystal, but due to the periodic structure, it is only at the Bragg angles the elastically scattered X-rays interfere constructively resulting in intense diffracted beam. Sometimes, e.g. powder diffraction, it is not possible to determine the orientation of the crystal. Instead the angle between the incoming and the diffracted beam is used, which is equal to 2θ, as seen in figure 6.5 (grey).

As described in section 6.1.2, the atoms can be seen as positioned in different parallel planes with the same distance between adjacent parallel planes. Each set of parallel planes with an adjacent distance will give rise to a diffracted beam according to Bragg's Law. Since all crystals have a specific structure, also the distance between adjacent parallel planes and the Bragg angles is specific for each crystal. This can be used to deduce the different crystal structures of a sample.

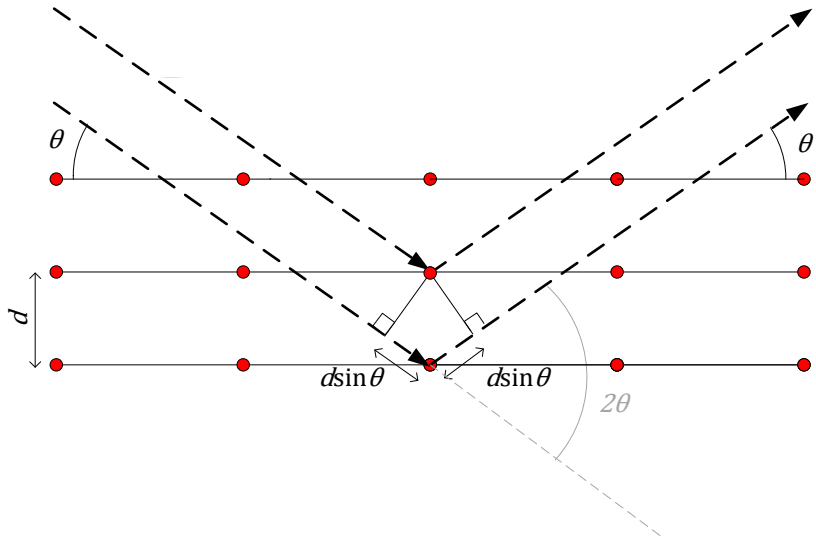

Figure 6.5. Diffraction from a crystal according to Bragg's Law. For the distance d and wavelength λ specific incident angle θ, the phase difference between scattered x-rays from each plane interferes constructively when the angle for the scattered x-rays is the same as the incoming.

6.1.4 Powder diffraction

One way of using X-ray diffraction is to measure the crystalline structure of a powdered sample. The powder sample, as the name indicates, consists of many small crystalline particles, called crystallites. These crystallites are large in an atomic scale, i.e. consist of enough many atoms (planes) such that they can yield well defined diffracted beams, but in the macroscopic scale is small. This means that a macroscopic sample (~mm) can approximately consist of infinitely many small crystallites.

Further, the crystallites does not have a preferred orientation (approximately) and are therefore randomly oriented relative to each other, as illustrated in figure 6.6 for one set of parallel planes. If X-rays irradiate the sample, diffracted beams are achieved from the crystallites that are oriented correctly (red), which is when the X-ray incidence the planes according to the Bragg angle.

In the example, only one set of planes were considered, where diffracted beams were achieved from only a fraction of the crystallites. The other crystallites are most probable oriented correctly to get diffracted beams from a other set of the parallel planes (as they have other Bragg angles), but not the same set of planes for all crystallites, such that it is at least a fraction of crystallites are oriented correctly for every set of parallel planes. Hence, the diffracted beams from all crystallites together show all the possible diffracted beams from the crystals in the sample.

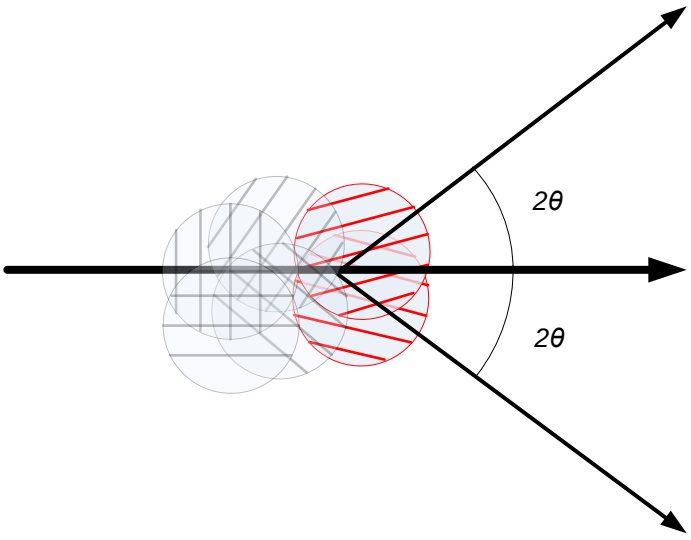

Figure 6.6. Illustration that shows the diffraction from one set of parallel planes in a powder. It is only a fraction of the particles (red) that are oriented correctly such that diffraction is achieved from that set of planes.

In the 2-dimensional example in figure 6.6, there are two possible orientations (red) for the particles such they provide diffracted beams upward and downward, respectively, with a diffraction angle 2θ. If considering 3-dimensions, the diffracted beams from one set of parallel planes is spread into a Debye-Scherrer cone, as seen in figure 6.7. All the Debye-Scherrer cones from the crystal are usually detected as a projection onto a flat plane detector. The pattern recorded by the detector consists of so-called powder rings, where each ring corresponds to a distance between parallel planes.

In this project, the 2-dimensional detector image is integrated circularly to achieve a diffractogram, where the intensities of the rings are shown as peaks at different 2θ angles, as illustrated in figure 6.8. The calibration and the integration are usually handled automatically by the use of standardized calibrant samples and softwares, for example FIT2D [18].

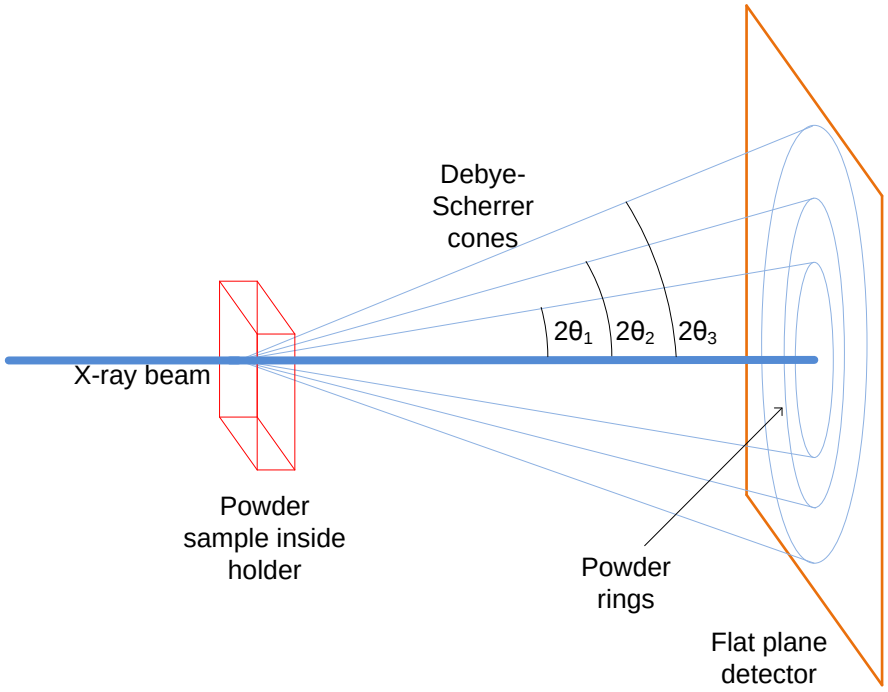

Figure 6.7. Illustration of how the X-rays are diffracted at the powder into so called Debye-Scherrer cones, which are projected onto a flat plane detector as so called powder rings.

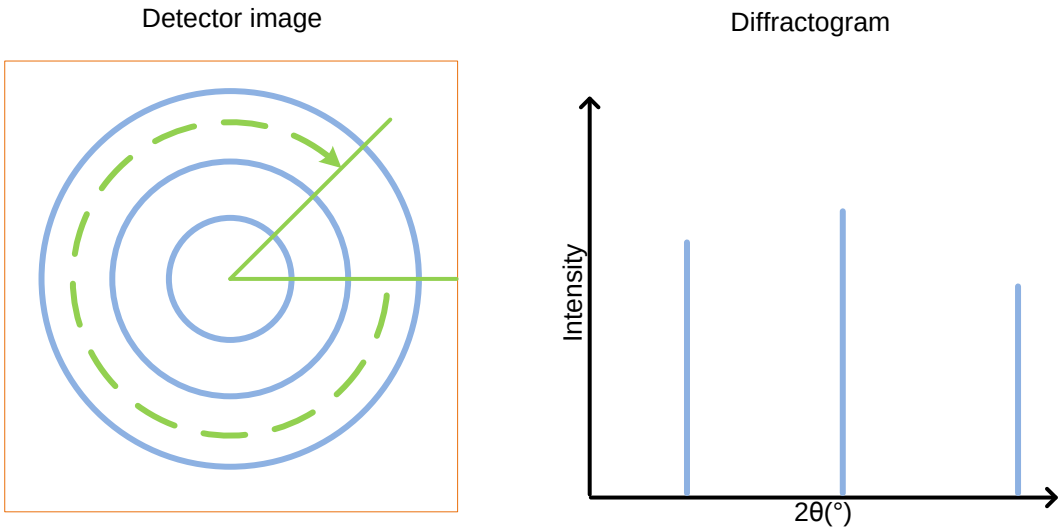

Figure 6.8. Illustration of how the detector image is circularly integrated to give a diffractogram with peaks.

6.2 Mass Spectrometer

The quadrupole mass spectrometer (QMS) is widely used for chemical analysis of gases and is the most common method to measure relative amount of different species (molecules) in the gas during heterogeneous catalytic processes.

The main parts of a QMS are an ion source that ionizes the molecules, a quadrupole mass filter (QMF) that filters out a mass to charge ratio and a detector that counts the amount of mass to charge ratio that has passed the filter [19]. The relative amount of species in the gas is measured by leaking a small fraction of the gas into the QMS. The leaked in gas goes through the parts from left to right as seen in figure 6.9.

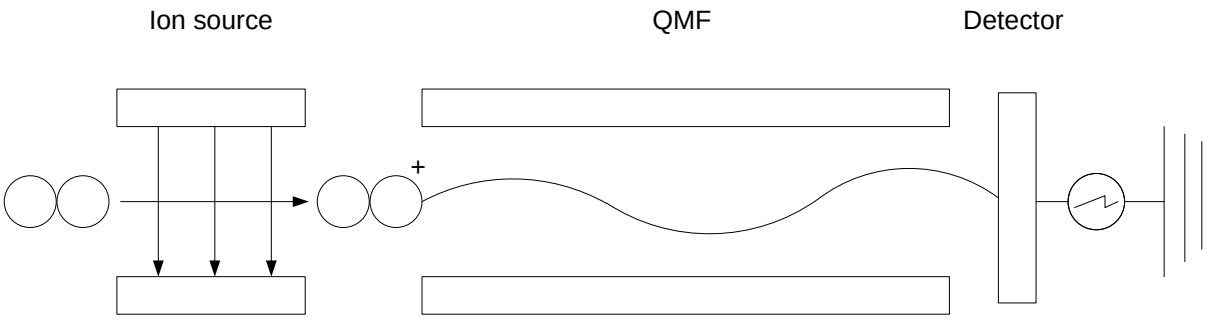

Figure 6.9. Illustration of the different parts of the QMS.

The ion source consists of a cathode and an anode creating an electric field between them. The cathode is heated to start emitting electrons that will accelerate towards the anode. In the ion source, the different molecules will be positively ionized by the electrons and can also collide with each other. These processes crack the molecules into different ions with different mass to charge ratios.

After the molecules have been ionized, they proceed into the QMF, which consists of four parallel electrodes with the ends forming a square as shown in figure 6.10. Two of the rods are connected to the mostly negative part and two are connected to the mostly positive part of a bias, which consists of both a DC and AC voltage.

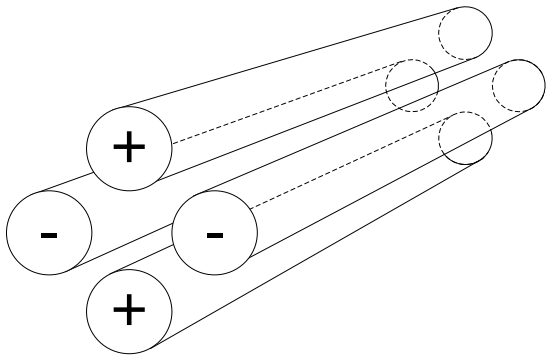

Figure 6.10. Illustration of the quadrupole mass filter.

The result is an electrical quadrupole field between the rods. The path of different ions, through the QMF will be affected according to the alternating voltage and their mass to charge ratio [20]. If the DC part is zero, the effect on the ions will be equal from the

alternating positive and negative voltage. The positive ions will therefore be accelerated towards the electrode when the voltage is negative and towards the centre axis when the electrode is positive. If the ion mass to charge ratio is low enough or the time the electrodes are negative is long enough, the ions will hit one of the electrodes, discharge and not pass through the filter.

By adding the DC part the total voltage oscillation will be around another position than zero. The two electrodes with positive DC voltage will have longer time with positive voltage and shorter time with negative voltage, if the amplitude of the AC voltage is higher than the DC voltage. In this situation ions with high mass to charge ratio will not have the time to accelerate before the AC voltage changes sign and therefore stay in the middle of the quadrupole field and the two electrodes. These two electrodes will therefore only allow ions with high enough mass to charge ratio to pass the filter.

The other two electrodes will have the same DC voltage but with changed sign and the AC voltage half a period off relative the other two more positive electrodes. They will only allow the ions with low mass to charge ratio to pass the filter, because they do not have time to accelerate during the short time of negative voltage.

The voltage can be set to act as a band pass filter for the ions only allowing one mass to charge ratio to pass. In figure 6.11 the paths of three different ions are illustrated. In (a) is the path of an ion with too low mass to charge ratio, in (b) is the mass to charge ratio too high and in (c) the same ratio as the one that are allowed to pass.

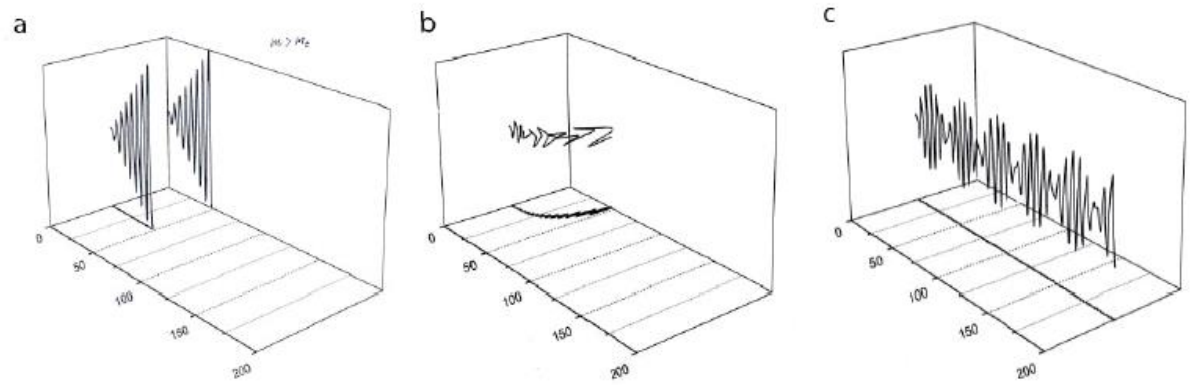

Figure 6.11. Illustration of the paths for three different ions in the QMF. In (a) is the path of an ion with too low mass to charge ratio, in (b) is the mass to charge ratio too high and in (c) the same ratio as the one that are allowed to pass. [21]

In the final step, the ions that pass the filter are counted by the detector. The detector can in the simplest case be seen as a plate where the ions hit and leave their charge. The number of ions that hits the plate is deduced by measuring the current that is generated as the plate discharges. The detector is usually either a Faraday cup or secondary electron multiplier. The advantage of the latter is that it amplifies the signal before it is measured, which makes it possible to measure smaller quantities of molecules.

In the QMS, the molecules are ionized with different probabilities and cracked into a set of different mass to charge ratios, which is called a cracking pattern. Both the ionization probability and the cracking pattern are specific for each molecule, which means that it can

be used to distinguish between different kinds of molecules in the gas. If these parameters are known it is possible to deduce the relative concentration of species in the gas.

6.3 Planar Laser Induced Fluorescence

Laser Induced Fluorescence (LIF) is a common method for concentration measurement of the different species in gases e.g. in combustion physics, but it is not widely used in heterogeneous catalysis research. One of the advantages the LIF method has compared to mass spectrometry is that it is possible to measure the concentration locally in for example a reactor cell.

An evolution of LIF is Planar LIF (PLIF), where it is possible to deduce the distribution of the species in a gas over two dimensions, which allows for live comparison of the gas distribution in the probed area. This method has before been used to measure the concentration of OH and formaldehyde formed over catalyst [22, 23]. However, for CO_2 formed over catalysts from for example CO or CH_4 oxidation, less reports exists [24]. This is mostly due to the problems of thermal background and inaccessibility of lasers and detectors that are needed to perform the measurement. Below follows a short description of the PLIF method. A more extensive description can be found in reference [25].

Figure 6.12 illustrates the principle of how the PLIF method is used to measure the species of interest in a gas cloud. The species of interest are the molecules in the gas, which concentrations are of interest. The laser beam is sent through a set of lenses to form a 2-dimensional laser sheet, which propagates through the gas cloud. By tuning the wavelength of the laser to match a transition in the species of interest, the molecules can be excited, as shown in figure 6.13 (thicker arrow). After a short time, they will spontaneously relax by sending out fluorescence (thinner arrows) in all directions. If the fluorescence is recorded with a two dimensional camera placed perpendicular to the laser sheet, the recorded image yields the distribution of the probed molecules.

If the laser and the fluorescence are in the IR-region, as it was for the measurements in this project, there is a problem with a high background due to heat. This problem can be minimized by doing two recordings. The first as the laser is on and the second when the laser is off, which measures the background. By subtracting the second from the first recording, a background free image of the concentration of species of interest is achieved. The setup used in this project yielded a background free image every 0.1 s, limited by the 10 Hz repetition rate of the laser (the camera repetition rate was set to 20 Hz), and a spatial resolution of 400 µm.

When choosing which transition the laser should excite, it is important to take into account two factors. The first is that the wavelength should excite a transition only in the species of interest and no other species in the probed volume, as they also will fluorescence if excited and make it difficult to distinguish between the different signals. The second effect that must be taken into account is related to the population of the probed energy level, i.e. the energy level the molecules gets excited from. The population of the energy levels is described by the Boltzmann distribution, which means it depends on the temperature. Since different energy levels are affected to different extent, it is possible to minimize the effect by choosing the transition that is affected the least. Even if the effect is minimized it is not possible to completely remove it. Hence, it should also be taken into account when analyzing the data.

Another temperature dependent effect that should be taken into account is related to the number of molecules, which follows the ideal gas law

$$n = \frac{PV}{k_B T},$$

where n is the number of molecules, P is the pressure, V the volume, k_B the Boltzmann constant and T the temperature. The law shows that if the temperature increases, while the volume and the pressure are kept constant, the number of molecules decreases linearly. This means that the number of species of interest and consequently also the intensity of the fluorescence is decreased.

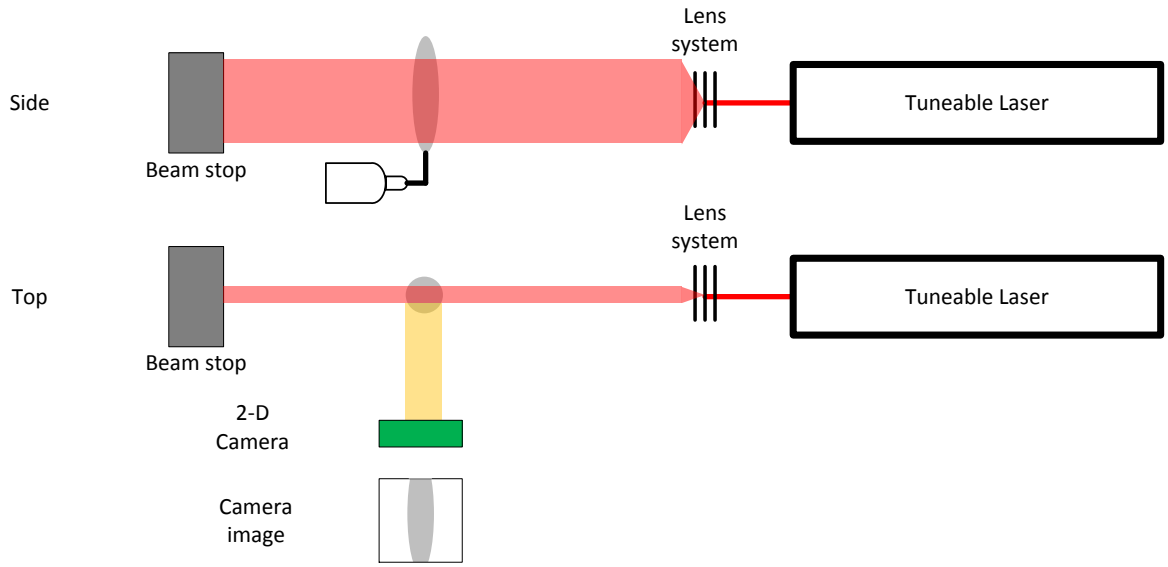

Figure 6.12. Illustration of the planar laser induced method seen from the side and top.

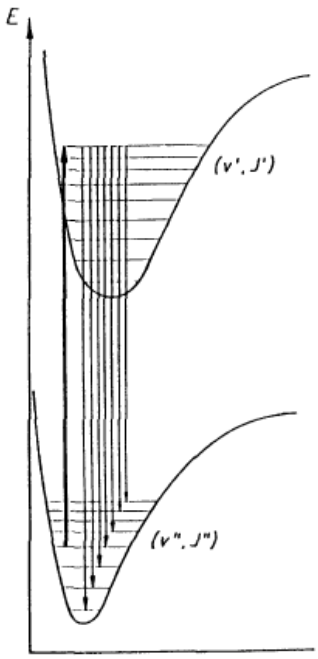

Figure 6.13 Illustration that shows the transition involved in LIF. The molecules are first excited to a higher energy level (thicker arrow) and after a while they relax by sending out fluorescence (thinner arrows). [38]

7 Common setups

This section introduces the common setups used in all of the experiments. The chapter is organized into two sections; 7.1) Gas system and 7.2) Temperature.

7.1 Gas system

During the project different gas mixtures were flown through the reactors. It is important to set the flow rate through and the pressure in the reactor accurately and in a convenient way. To do this a gas system that consists of several flow and pressure controllers is used. The controllers were provided by Bronkhorst [26].

Figure 7.1 is an illustration of the gas system. It consist of five flow controllers that can let 1-50 ml_n/min (1 mln =1 ml at standard (normal) pressure and temperature) of a certain gas through each controller and one pressure controller that can control the pressure in the reactor between around 0 - 1000 mbar. The direction of the gas flow is controlled by five electronic valves, ten manual screw valves and five manual mechanical valves [27]. The five flow controllers make it possible to mix five different gases with a ratio of between 2 % / 98 % to 50 % / 50 % for two of the gases. The pressure controller makes it possible to do flow measurement with a specific pressure in the reactor and the valves and the pressure controller closest to the reactor can be closed for experiments in batch mode. It is also possible to pump the reactor from several directions. The gas system is mobile and easy to attach, which makes it possible to use with many different reactor.

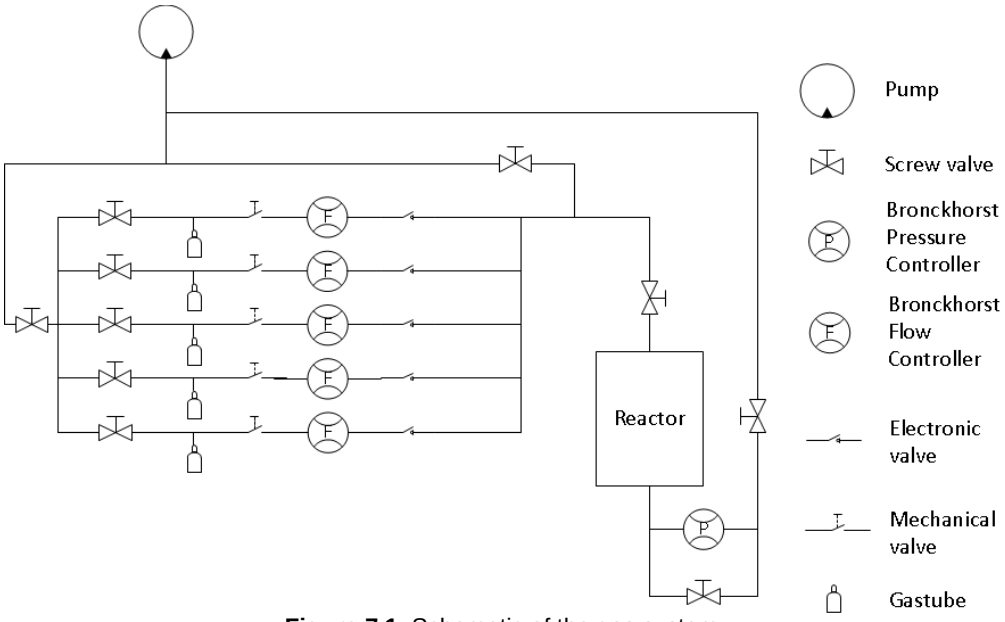

Figure 7.1. Schematic of the gas system.

7.2 Temperature

Except the flows also the temperature of the catalyst is important to set accurately. This section introduces the way the reactors were heated and how the temperature was measured.

7.2.1 Heating

In this project all the catalyst were heated using resistance heating wires, which produce heat when a current goes through the wire. The produced heat and thereby also the temperature are controlled by the current. The heating wires were of Kanthal, which is an alloy of iron-chromium-aluminum that can be used as heating element up to 1300°C [28].

7.2.2 Measure

The temperature was measured using thermocouple wires. A thermocouple consists of two metallic wires of different materials, which is joined at the place where the temperature should be measured. The different materials respond differently to temperature and a potential difference is induced between the wires. By measuring the potential difference it is possible to deduce the temperature.

There exist many different types of commercial thermocouples that are calibrated, for showing temperature, in advance. The accuracy of these thermocouples are around 1-2°C. The different thermocouples have different properties, which makes them less or more useful for measurements in catalytic reactive conditions. In this project the thermocouple type K was used.

8 Reactor design and case studies

In this chapter the design of the different reactors together with the case studies performed with the reactors is described. The different descriptions with cases are organized into three sections: 8.1 Flow reactor measurements, 8.2 Reactor for activity measurements of three catalysts simultaneously and 8.2 XRD measurements.

8.1 Flow reactor measurements

This section describes the design of the flow reactor used for activity measurements using mass spectrometry. The reactor was tested with case studies of CH_4 oxidation over Pd and PdAg foils. Flow reactor measurements offer a comparably cheap method for testing several catalysts under different conditions. The method lacks the possibility to directly follow the structure of the catalyst or the gas distribution close to the sample. Instead the gas is analyzed first when the gas has passed the catalyst and the reactor. By comparing the results with other measurements, however, it is possible to couple the gained information to structural changes in the catalyst. The section is organized into three parts: 8.1.1 Setup, 8.1.2 Higher temperature measurements, 8.1.3 Lower temperature measurements.

8.1.1 Setup

Figure 8.1 and 8.2 show a photo and a schematic illustration of the reactor with setup. The reactor is a 1000 mm long Quartz tube with 9 mm outer diameter and 7 mm inner diameter.

The reactor is heated by a resistance heating wire of Kanthal coiled around the tube and the temperature measured with a type K thermocouple inserted into the reactor through a feedthrough. In order to avoid heat leakage, and distribute the heat more evenly over the reactor, the tube and heating wire is wrapped with quartz wool, which is kept fixed by aluminum foil. Hence the heating wire is not visible in figure 8.1.

The gas system described in section 7.1 was used to control the gas flow through the reactor. The tube is connected to the gas line using reusable Ultra-Torr Vacuum fittings that uses rubber O-rings for sealing [27]. After passing the reactor, the gas is analyzed with a QMS.

During the measurements the sample was placed in a monolith, which worked as holder. The thermocouple end was placed in one of the holes of the monolith and measured the temperature close to the sample.

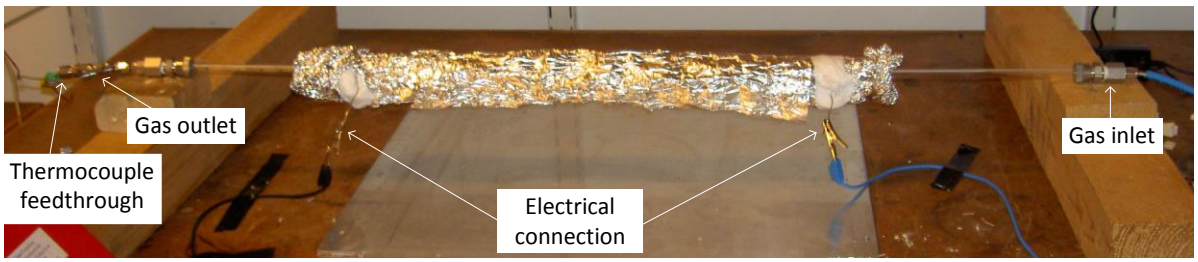

Figure 8.1. Photo of the reactor.

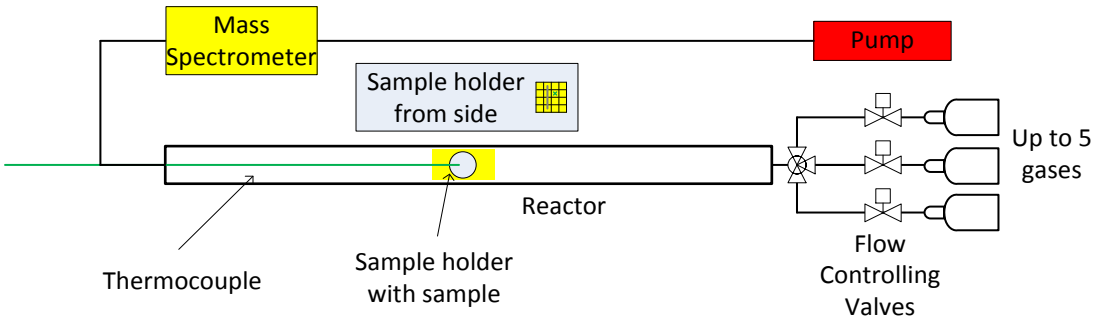

Figure 8.2. Illustration of setup.

8.1.2 High temperature measurements over foil samples

This section reports the results from the higher temperature measurements of CH_4 oxidation over Pd and $Pd_{70}Ag_{30}$ (alloy of 70 % Pd and 30 % silver, hereafter called PdAg). The Pd foils are in the shape of round thin disks with a diameter of 6 mm and thickness of 0.1 mm. The PdAg foils, which were not available as disks, were cut in a similar size. Both of them were provided by [29].

Figure 8.3 illustrates the way both the foils were studied. Three consecutive sets (1-3) of measurements were performed over each sample, in which the gas flow was oxygen rich in set 1 and 3 and methane rich in set 2. The flows are explicitly written in the figure. The oxygen and methane rich flow promotes complete or partial oxidation of methane, respectively. The O_2 and CH_4 were both diluted with 95 % Argon (Ar) in the gas bottles before use. Hence, the starting conditions in 1000 mbar were 13 mbar CH_4, 37 mbar O_2 and 950 mbar Ar for the oxygen rich flow, and 38 mbar CH_4, 12 mbar O_2 and 950 mbar Ar for the methane rich flow. Ar is used since it is chemical inert and does not share the mass with any other molecules in the measurement. This is preferable since molecules with the same mass are partially detected at the same mass to charge ratio in the MS.

Three temperature ramps (a-c) were performed in each set, where every temperature ramp started and finished at 300°C and peaked at 900°C. The heating/cooling speed was 0.4°C/s for every ramp.

		Set 1	Set 2	Set 3
Gas mixture (ml_n/min)		CH_4 = 0.9 O_2 = 2.5	CH_4 = 2.3 O_2 = 0.7	CH_4 = 0.9 O_2 = 2.5
Temp	Pd			
	PdAg	a b c	a b c	a b c

Figure 8.3. Illustration of how the measurements were performed on both the Pd foil and the PdAg foil. Three sets (1-3) were performed over each sample. The first and third using oxygen rich flow, the second using methane rich flow. Three temperature ramps (a-c) were performed in each set.

8.1.2.1 Result

The presentations of the interesting results from the measurements are organized into four sections: 8.1.2.1.1 General behavior on the CO_2 production under oxygen rich condition, 8.1.2.1.2 Methane rich condition, 8.1.2.1.3 Spontaneous reaction oscillations, 8.1.2.1.4 History of the sample and 8.1.2.1.5 Comparison between Pd and PdAg.

The results are shown, unless otherwise stated, as the production of CO_2 at different temperatures of the ramp. The production is plotted as the percent of how much CO_2 that can possible be produced. 100% means that all CH_4 has been converted to CO_2 according to the complete methane oxidation scheme. The ramps are denoted according to which set the ramp is performed (1-3) and which ramp in the set (a-c). For example denotes ramp 2a, temperature ramp a in set 2.

8.1.2.1.1 General behavior of the CO_2 production in oxygen rich flow

This section describes a typical experiment over a Pd foil, where complete oxidation of methane to CO_2 and H_2O was studied under oxygen rich conditions during a temperature ramp. This measurement should be compared to single crystal Pd(100) results from similar conditions by Hellman et al [11]. This study was discussed further in section 5.5, but the main result was that four different phases of Pd were identified during the temperature ramp. The metallic surface that is active, an ultra-thin surface oxide that is inactive, an epitaxial bulk oxide (at least two layers thick) is possibly even more active than the metallic surface, and a thick oxide is inactive. Over the crystal surface it was seen that the active oxide is present up to about 500°C, where instead the inactive oxide takes over and is present until the surface turns metallic and active after 570°C.

Figure 8.4 (a) shows the CO_2 production over the Pd foil during ramp 1b. Here the activity is low up to about 600°C, where something happens and the surface turns active until about 690°C. Above 690°C the activity goes down and over 800°C it is active again.

If comparing the low temperature region, up to 600°C, with the single crystal measurements, it seems like the foil is, since the activity is low, in the inactive oxide phase already in the beginning of the ramp. This interpretation is confirmed by the Arrhenius plot in figure 8.4 (b), where the linear behavior between inverse temperatures of 1.7 and 1.15 1/K (about 300-600°C) indicate that the activation energy does not change over this temperature range, i.e. there is no phase transition from the active to the inactive oxide. At about 600°C, the temperature is high enough in order for the oxide to desorb from the surface, leaving the catalyst in a metallic active phase.

Above 690°C, however, the CO_2 production drops with increasing temperature, in contrast to the usual temperature dependence of chemical reactions. This is most probably due to faster desorption than adsorption of reactants on the catalytic surface. As the reaction takes place when the reactants are at the surface, the catalytic activity must consequently go down.

The CO_2 production stays low until the temperature reaches 800°C, where CO_2 production increases very suddenly. Above this temperature, the same conversion is found even without a catalyst in the reactor. Hence we conclude that the reaction at high temperature is non-catalytic.

When the temperature is ramped down from 900°C (red), we first note that the temperature for where the non-catalytic reaction is found is slightly shifted towards lower temperature. This is explained by the experimental error due to the time delay between the temperature measurement, which is done in the middle of the tube, and the gas analysis, which is done when the gas has passed the reactor and got into the QMS.

Further down in temperature, the CO_2 production stays low over a remarkably large temperature range, and not until below 600°C, the activity is as high as for the ramp up. The

low production between 650°C and 750°C indicates that there must be another in-active phase, which is present over the temperature range, where the active metal was present during the up ramp. Graphene can be formed by exposing noble metals to hydrocarbons (such as C_2H_4) at around 900°C [30]. This could be the same for CH_4. Hence, the inactive phase could be due to a graphene film, which is almost totally inert and blocks the surface from being oxidized. Not until about 600°C enough oxygen can be pushed on to the surface in order to break the film and leave the surface in the more active but still rather inactive oxide phase.

This brings us back to the up ramp, where there was a thick inactive oxide already at the start. This oxide must have formed during the previous down ramp. As will be seen below, this is not the case when the temperature during the ramp did not go above 650°C. At this lower temperature, the graphene layer does not seem to form either. Hence, it seems like the Pd oxide, when formed in conjunction with the removal of the graphene layer, growth directly to the thick inactive film, while without the graphene, the oxidation is slower and stops with the thinner active film. The exact mechanism behind this is presently unknown.

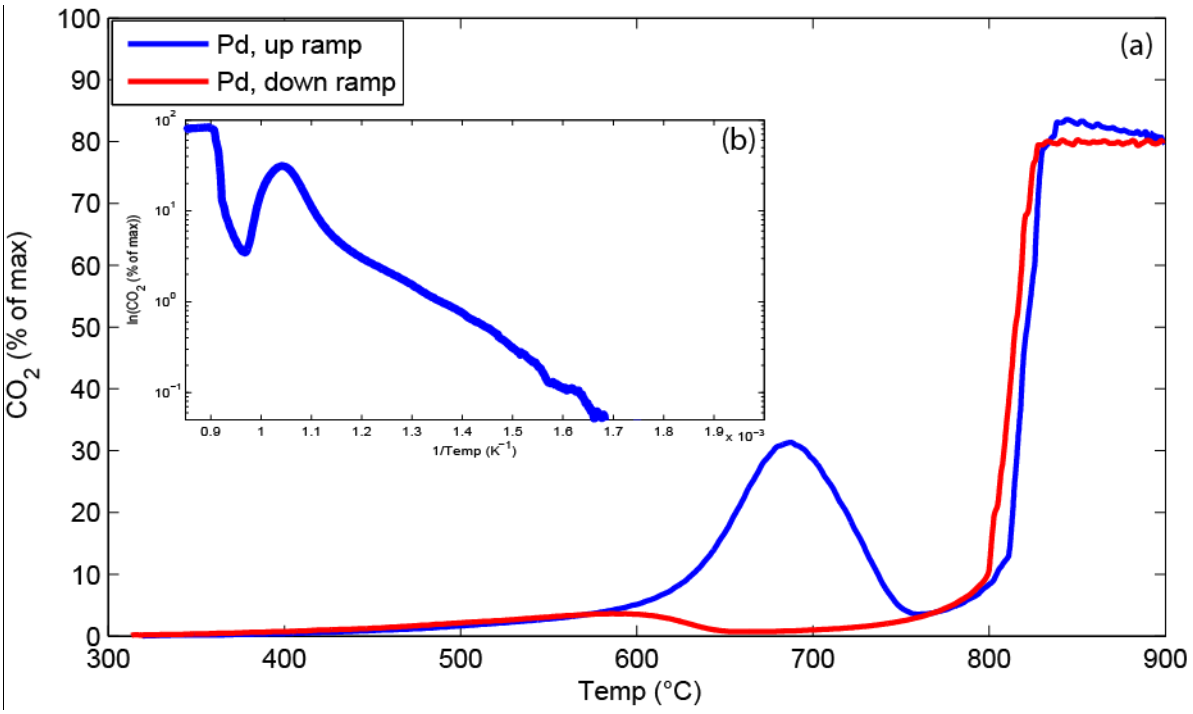

Figure 8.4. (a) CO_2 production over the Pd foil under oxygen rich conditions during ramp 1b. (b) Arrhenius plot of the CO_2 production during the temperature increase in (a).

8.1.2.1.2 Methane rich flow

In an excess of methane it is possible to run the partial oxidation of methane, giving CO and H_2 as products. A gas mixture of CO and H_2 is referred to as syngas, which in turn is used to produce different hydrocarbons through the Fischer-Tropsch process. Since the partial oxidation competes with the complete oxidation path, it is of interest to develop catalysts and methods for promoting the partial oxidation.

This section shows the result from the measurement over the Pd foil using the methane rich flow. As with the oxygen rich flow, the measurement over PdAg shows similar results, but with generally lower production.

Figure 8.5 shows the results from ramp 2b over the Pd foil. It shows that below 500°C mainly CO_2 and H_2O are produced, according to the complete oxidation path. At 500°C there is a significant increase of the CO production, which continues with further increase of the temperature. At the same time, the CO_2 production decreases. For the hydrogen containing products, both H_2 and H_2O rises with CO at 500°C. At higher temperature, the H_2O is rather constant while H_2 increases steadily. Not until 800°C, though the H_2 signal passes the H_2O signal.

For an interpretation of this data, we look at the amount of oxygen that is found at the surface. At lower temperature the surface is probably oxidized. This means that the surface has an excess of oxygen, which promotes the complete oxidation process, i.e. more CO_2 and H_2O is produced. As the temperature is increased the oxide desorbs and the surface becomes metallic. This phase transition is known to occur at about 500°C - 600°C (under oxygen rich conditions it happens at higher temperature due to higher oxygen pressure), and above this temperature, the conditions on the surface is more similar to the conditions in the gas phase, i.e. methane rich, which promotes partial oxidation of methane.

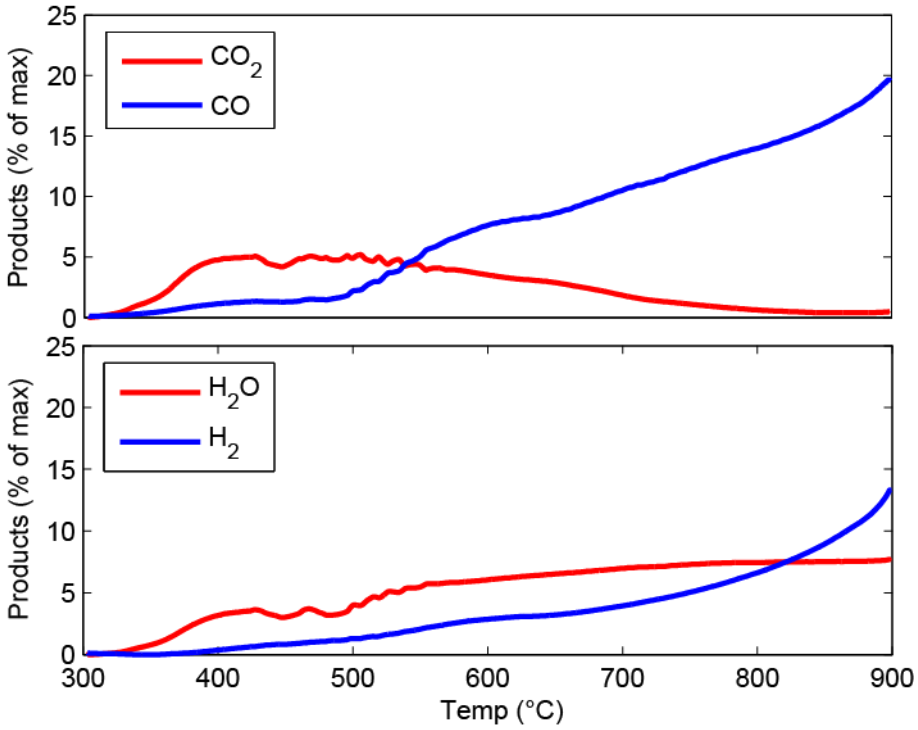

Figure 8.5. Production over the Pd foil under methane rich conditions during the temperature increase of ramp 2b.

8.1.2.1.3 Spontaneous reaction oscillations

During the measurements with methane rich flow, such as in figure 8.5, the CO and CO_2 signals starts to oscillate, seen in figure 8.5 at around 500°C. The signals oscillate such minima in the CO_2 signal correspond to maxima in the CO signal, and vice versa. By stopping the temperature, the oscillations can be kept going for longer time (at least several minutes), as shown in figure 8.6 where the temperature is kept constant at 550°C.

The oscillations are related to a phase transition between a methane and an oxygen rich surface. When the surface is oxygen rich, the O_2:CH_4 ratio is high at the surface such the CH_4 is oxidized through the complete reaction path. As the complete reaction uses two O_2 molecules for every CH_4 molecules, the O_2:CH_4 ratio decreases as the reaction runs.

When the O_2:CH_4 ratio is low enough the oxygen cannot keep dominating the surface, and the surface turns methane rich. In this phase the relative concentration of oxygen and methane at the surface is more similar the concentration in the gas. This means that the partial oxidation is promoted, and since this reaction uses two CH_4 molecules for every O_2 molecule, the O_2:CH_4 ratio increases again. Finally, oxygen reclaims the surface, and the CH_4 is oxidized through the complete reaction path again.

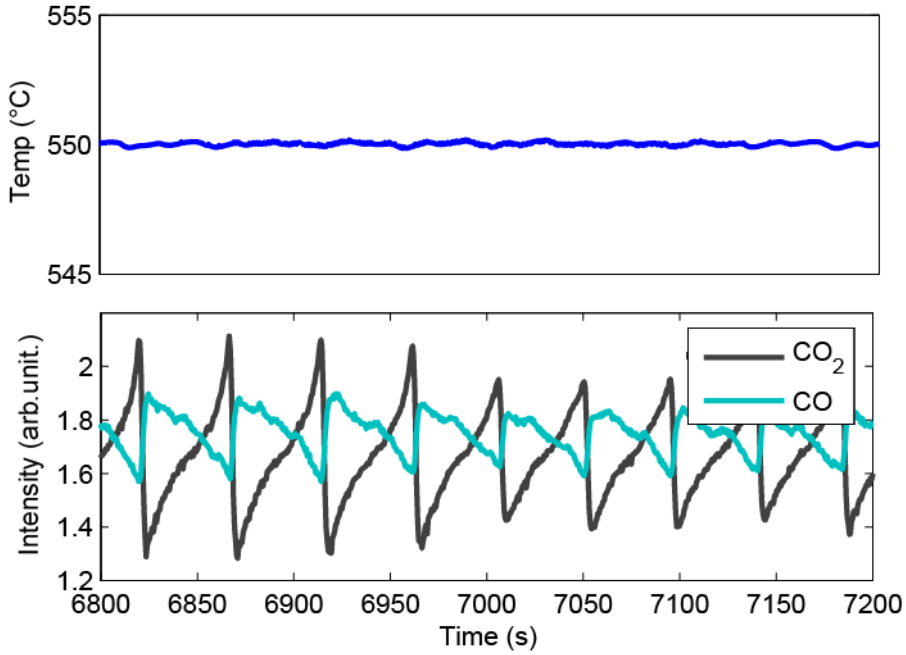

Figure 8.6. Spontaneous reaction oscillations of the CO_2 and CO signals under methane rich conditions over the Pd foil at constant temperature of 550°C.

8.1.2.1.4 History of the sample

When returning to the oxygen rich flow, in set 3, the CO_2 production is quite different as compared to set 1. Also between the ramps in each set the production is different. This section deals with the differences in CO_2 production between the different ramps in set 1 and 3, i.e. how the history of the sample affects the production. Figure 8.7 shows the CO_2 production during heating of ramp 1a (blue) and ramp 1b (red) in set 1 and ramp 3a (green) and ramp 3b (black) in set 3.

For ramp 1a, the production increases almost linearly between 300°C and 660°C. In general the speed of a certain reaction increases exponentially with temperature. Hence the linear behavior in ramp 1a suggests that there is a gradual phase change towards lower activity. This is confirmed by the following ramp 1b, which reveals a CO_2 production that is constantly lower. Furthermore, the temperature dependence is now close to exponential. A possible explanation of what has happened can be found by looking at how the surface changes during ramp 1a.

When the foil is new, its surface is probably rather rough. A rough surface provides a larger surface area and hence shows a higher activity than a flat surface. We therefore explain the difference between the first two ramps with the surface being rougher during ramp 1a than during the following ramp 1b. As the sample is heated, the atoms gets more mobile, such that they can rearrange themselves to minimize their energy. Since surface area is energetically unfavorable, this can be achieved by making the surface smoother. The next ramp 1c (not plotted here) yields similar results as the second ramp. Probably the surface

area is minimized almost completely after the first ramp 1a such that the area cannot be decreased further.

After the methane rich measurements (set 2), the ramps in set 3 yields a significantly higher CO_2 production. This is especially true for the first ramp 3a, where the CO_2 production increases quickly between 300°C and 450°C, then almost flattens out before an additional CO_2 production peak is seen between 530°C and 570°C.

It is known that in a methane rich environment, as in set 2, it is possible to form Pd carbides. The carbide is also known to increase the roughness of the surface and thereby the surface area [31]. The larger surface area explains why ramp 3a yields a generally higher CO_2 production, but not the additional peak between 530°C up to 570°C.

Figure 8.8 shows the CO_2, O_2 and CH_4 signals for the same temperature ramp. The signals are scaled such that the CH_4 and O_2 signals follow each other if the reaction follows the complete oxidation scheme. The O_2 and CH_4 signals do indeed follow each other except, between 600-750 s where a peak is found in the CO_2 signal. The production of CO_2 without a corresponding consumption of CH_4 can be explained by the release of carbon from the carbide, with which the oxygen reacts. The carbide is rather stable and does not decompose until the temperature has reached 530°C, and not until 570°C it is completely removed.

During the next ramp 3b, the CO_2 production increases almost linearly again, which is probable as the surface can be rough even after the carbide has disappeared.

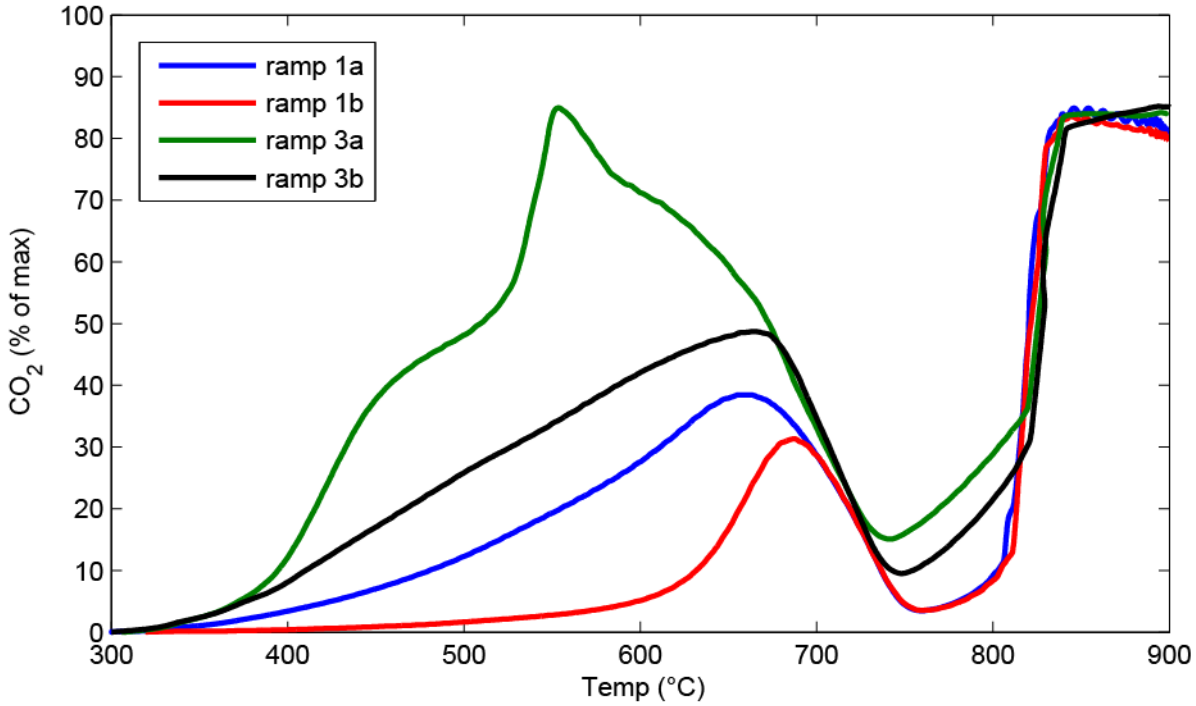

Figure 8.7. Comparison of the CO_2 production under oxygen rich conditions over the Pd foil for the increase of four temperature ramps. Note the differences before 700°C.

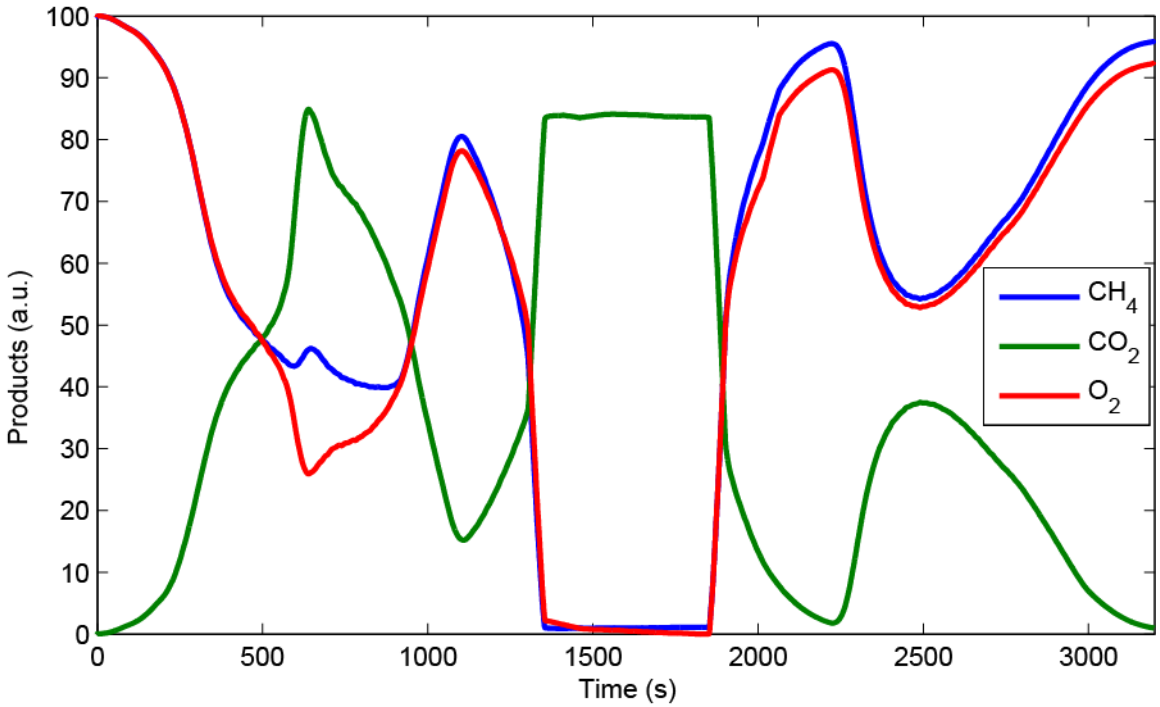

Figure 8.8. The CO_2, O_2 and CH_4 signals for ramp 3a. The O_2 and CH_4 are scaled to follow each other if they only react with each other through the complete methane oxidation scheme. Note that the O_2 is consumed more than CH_4 between 500 s and 900 s, which indicate that O_2 reacts to CO_2 in another process than the complete oxidation process.

8.1.2.1.5 Comparison between Pd and PdAg

This section takes up the differences between the result from the measurement over the Pd and the PdAg foil. The PdAg is investigated to see the effect of silver in the sample. If it is possible to get the PdAg to be as active as pure Pd, it could be a way of doing cheaper catalysts with less of the expensive Pd. A way the PdAg could be as active as the pure Pd is if the Pd segregates to the surface of the alloy, such that most of the surface consist of active Pd.

The differences between the Pd and PdAg are presented using the result from ramp 1b for both the measurement over the Pd and the PdAg foil as an example, in which the important conclusions are seen. The result from the up ramp over both the Pd (blue) and the PdAg (red) is plotted in figure 8.9.

As the temperature increases, the CO_2 production for both samples increases, until 690°C or 700°C is reached for Pd and PdAg, respectively. Notably, the conversion is significantly lower over PdAg than over Pd. This indicates that silver is present at, or near, the surface in a way that has a negative effect on the activity. This shows, that at least under these conditions, Pd is not segregating to the surface to the extent needed for the PdAg catalyst to be more, or at least, as active as pure Pd.

At higher temperature, the gas phase reaction takes places, which is measured by the thermocouple to start at different temperatures in the two measurements, but this is probably an experimental error. The gas phase reaction starts when it somewhere in the tube have reached high enough temperature, i.e. the highest temperature in the tube. As the temperature is not uniformly distributed in the tube, it can be that the temperature the thermocouple measure is lower than the highest temperature in the tube, which consequently inducing an experimental error.

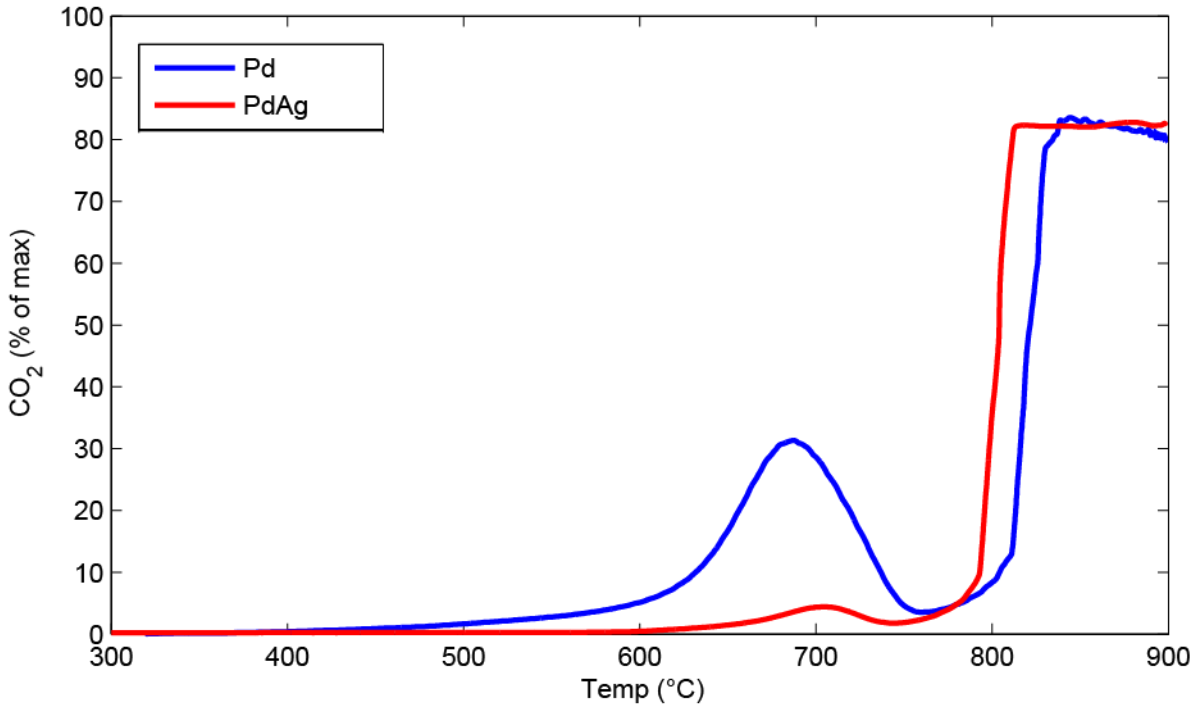

Figure 8.9. CO_2 production over the Pd and PdAg foils under rich oxygen conditions during the temperature increase of ramp 2b.

8.1.3 Low temperature measurement over Pd foil

As the experiments above failed to reproduce the single crystal results by Hellman et al [11], a new attempt was done where methane oxidation over Pd foil was studied during temperature ramps not higher than 640°C.

Figure 8.10 shows the production of CO_2 during a temperature ramp that started and finished at 300°C and peaked at 640°C. The heating/cooling speed was 0.3°C/s for every ramp. The flow was 0.9 ml_n/min CH_4 and 2.5 ml_n/min O_2 and the pressure 900 mbar. The O_2 and CH_4 were both diluted with 95 % Ar in the gas bottles before use. Hence, the starting condition was 12 mbar CH_4, 33 mbar O_2 and 855 mbar Ar.

8.1.3.1 Increase of temperature

While increasing the temperature, the CO_2 production goes up almost linearly up to around 450°C. After 450°C, the production starts to flatten out slightly before it starts to increase again at around 490°C. We interpret this as three phases being present during the temperature ramp, marked in the figure as phase 1-3. Phase 1 is the active epitaxial oxide, phase 2 is the in-active thick oxide, and phase 3 is the metallic active surface, in agreement with the single crystal results. A significant difference can, however, be seen as the transitions between the phases are sharper in the single crystal case (see figure 5.6) than for the foil, which in turn means that the difference between active and inactive phases are clearer in the single crystal case and during the in-active phase the production even decreases with temperature. These differences are possible to explain from the differences between a foil and a single crystal.

If comparing the surface of a single crystal with that of a foil, the former is more uniform and consist of one crystal surface, while the latter is more non-uniform, containing several steps and other defects, and a lot of smaller crystals.

Over the defect free single crystal, an adsorbate structure formed under certain conditions generally covers the whole surface. Over the foil, on the other hand, the mixture of different surface orientations can stabilize different structures simultaneously under the same conditions [32]. Hence, the transition between active and inactive structures, during the temperature ramp, is more gradual over the foil surface, which is reflected in figure 8.10.

8.1.3.2 Decrease of temperature

During the temperature drop (red), the CO_2 production is higher than in the up ramp all the way down to 450°C. We interpret this as the surface being metallic down to this temperature. This is in strong contrast to the ramps to 900°C, where the surface got covered by an inactive graphene film, which when removed at 600°C was immediately replaced by an inactive oxide.

An explanation for this difference would be that when the graphene film is decomposed, it leaves the surface in a rough state that is easily penetrated by oxygen forming an oxide. During the low-temperature ramp, the metallic phase is always smooth and withstands oxidation more efficiently. When the surface is finally oxidized, the oxide that is formed is the ultra-thin inactive surface oxide, which explains why the CO_2 production is lower than in the up ramp at this range of temperatures. As the temperature further decreases, the surface oxide growths thicker and is finally transformed into the same oxide as in the up ramp. This explains why the production in the down and up ramp coincidence again.

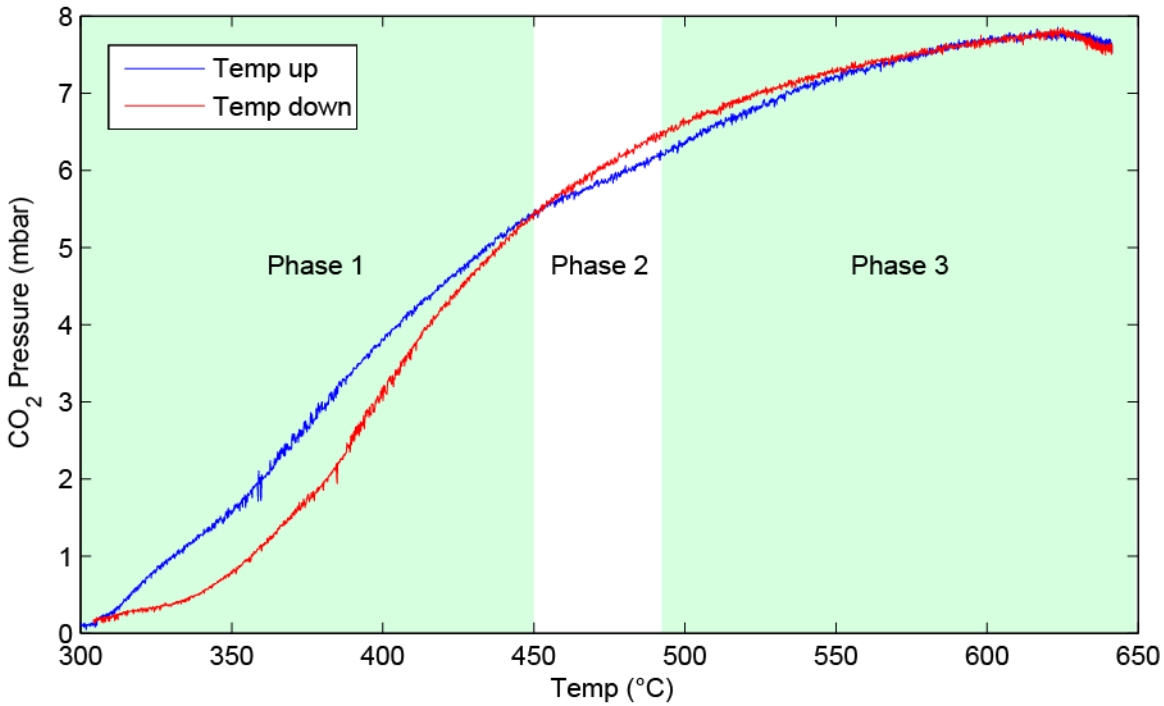

Figure 8.10. CO_2 production during the low temperature study of methane oxidation over the Pd foil. The production during the up ramp is divided into three phases (1-3).

8.2 Reactor for activity measurements of three catalysts simultaneously

This section describes the reactor used to measure the activity of three catalysts simultaneously using PLIF. Except the reactor design and the setup, a case study will be presented that shows the working principle of the method.

8.2.1 Setup

Figure 8.11 and 8.12 are an illustration and a photo of the setup used for the measurements. The main part is the reactor, which is a modified version of the flow reactor described in section 8.1, consisting of a larger quartz tube (black in the illustration) with three smaller quartz tubes inside (grey, only two is shown in the illustration). Inside each of the smaller tubes is one sample, which means that three catalysts can be tested simultaneously. The total length of the large tube with its CF16 ends is 500 mm and the inner diameter 16 mm. The smaller tubes are also 500 mm long but with an inner diameter of 5 mm.

As the flow reactor described in section 8.1, this reactor is heated by a resistance heating wire coiled around the larger tube, and quartz wool is wrapped around the coil in order to reduce heat leakage and get a more even temperature along the tube. The temperature is measured in the middle between the three smaller tubes with a type K thermocouple, which is introduced into the reactor by a feed through at the gas inlet. The gas mixture flows into the larger tube and is then split between the smaller tubes with the samples. In order to minimize the amount of gas passing between the smaller tubes, quartz fibres are used to block gap between the large tube and the small.

The reactor is connected to a CF40 cube with one of the CF16 ends of the larger tubes. The smaller tubes are pushed through the end of the larger tube into the centre of the cube. The gas mixture is after passing the reactor flown out of the ends of both the smaller and the larger tubes of the reactor into the CF40 stainless steel cube.

The gas is pumped out of the cube through the outlet at a corner of the cube and a small amount is leaked into a QMS. The pressure in the cube, and thereby also in the reactor, is controlled with a pressure controller after the QMS leak. The pressure is also measured with gauges at the CF40 cube. The gas system is described in section 7.1.

The laser system provides a tuneable infrared laser beam. It was shaped as sheet by a system of lenses before sent into the CF40 cube. The sheet went just outside the ends of the smaller tubes and the sheet covered the whole ends.

The laser was tuned to excite a transition in CO_2 without interference with transitions in other molecules. The line used was the rotational – vibrational line P (12) in the $(00^00) \rightarrow (10^001)$ transition.

The sheet therefore excites the CO_2 that flows out of the smaller tubes. When the molecules are deexcited, they send out fluorescence light in the IR region, which is detected with an IR camera at a right angle outside the cube. The laser beam and the fluorescence are allowed to pass in and out of the cube by the use of calcium fluoride windows.

The laser beam was repeated with a rate of 10 Hz while the camera recorded images at 20 Hz. This results in one image in sync with the laser and one background image out of sync with the laser. The background noise, which is mainly heat induced, can therefore be removed from the measurements, to give a background free image of the CO_2 concentration.

At high temperature, the thermal noise is, however, so high that it might result in a low signal to noise ratio after the background subtraction.

The CF40 cube is normally used as a reactor. In reference [24] that setup is explained in more detail.

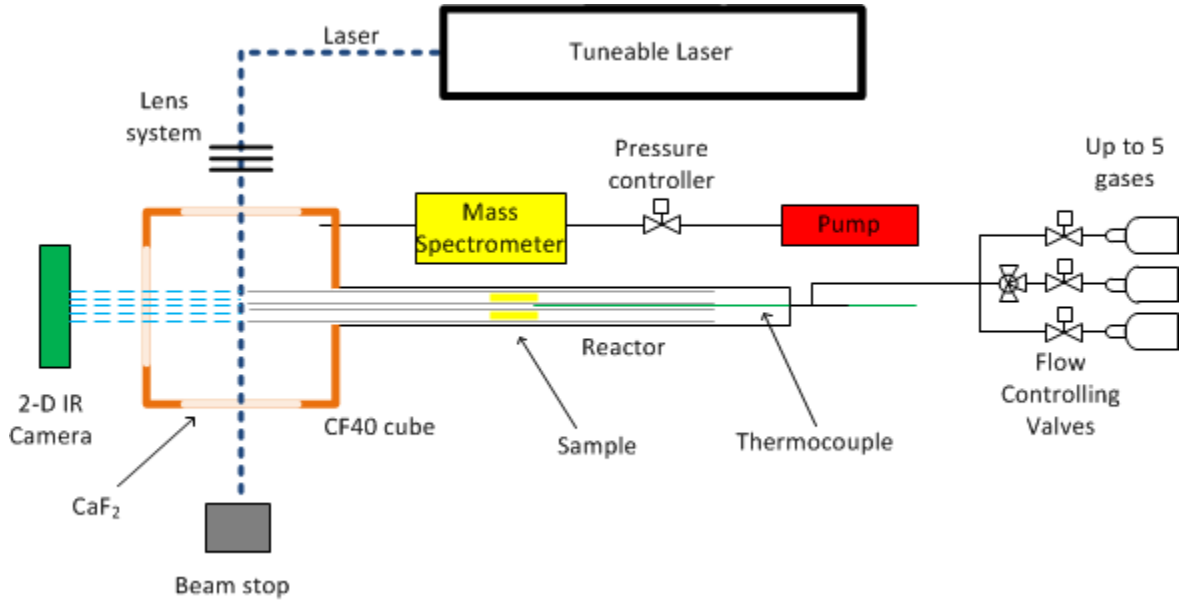

Figure 8.11. Illustration of the setup.

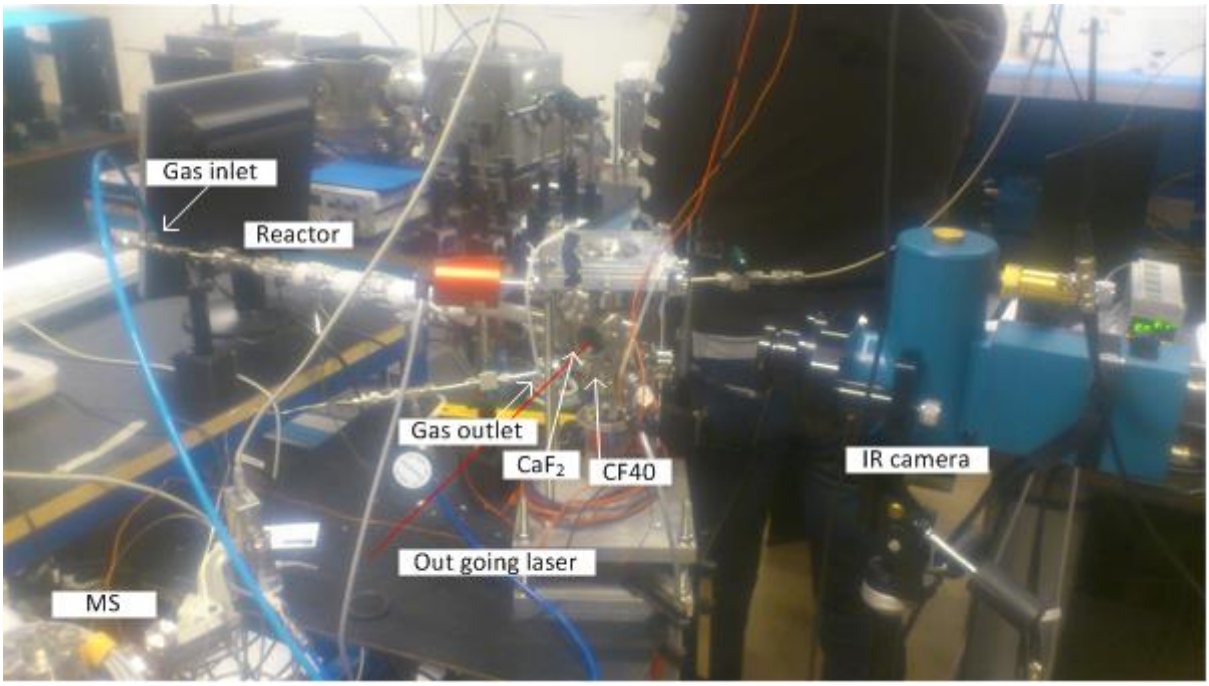

Figure 8.12. Image of the setup.

8.2.2 Reactor test

The reactor worked very well for CO oxidation studies, but for CH_4, which is significantly more difficult to oxidize, we had problems. The reason is probably that the diluted gas mixtures used (both the CH_4 and the O_2 were diluted to 5% in Ar) gave a too small amount of produced CO_2 in order to be detected, especially since the CH_4 oxidation reaction needs a

significantly higher temperature than CO oxidation, which results in a worse signal to noise ratio.

8.2.2.1 Result and discussion

Figure 8.13 shows a typical result from a measurement of CO oxidation. The flow was constantly 5 ml_n/min CO, 5 ml_n/min O_2 and 40 ml_n/min Ar at a constant pressure of 1000 mbar. Panel (a) shows images A)-D) recorded by the camera at the times indicated by the red lines in the plots. The higher intensity in A) that is shaped as round circles are artifact due to reflections from the smaller tube ends.

In each of the tubes is one monolith catalyst, which are very realistic or even the same as the catalyst used by the industry. A monolith is a ceramic multichannel structure of mostly cordierite. The monoliths used here consisted of 2×2 channels and were around 20 mm long and 3 mm thick. They were impregnated with three different catalysts. The monolith in the top tube was impregnated with Pt/CeO_2, the tube to the left with Pd/CeO_2 and the tube to the right with Pt/Al_2O_3.

Panel (b) shows the mean value of the intensity at the different tube ends. At every second ten images are averaged in order to increase the signal to noise ratio. Panel (c) shows the MS signal 44 (CO_2) and panel (d) the temperature.

As the temperature increases the different catalysts get activated at different temperatures and CO_2 is produced and flown out of the tube ends. In the recorded images A)-D) the activation of a catalyst is seen as more intensity outside the corresponding tubes. In plot (b) the entire activation process of each catalyst is possible to follow, which makes it possible to see which catalyst that is activated and to compare the activation process. In (c) the activation of the different catalysts is seen as an increase of the derivate in the signal, but it is impossible to deduce which catalyst that is activated.

The PLIF signal shows that Pd/CeO_2 is activated at lowest temperature, Pt/CeO_2 at a temperature in between and Pt/Al_2O_3 at the highest temperature. This is in agreement with previous results [33].

In the images, the higher intensity outside the tube is not centered on the end, but rather shifted downwards and to the left. This artifact must be due to the position of the gas outlet at a corner of the CF40 tube below the tubes as illustrated in figure 8.11. The CO_2 flown out of the tubes is probably directly going toward the direction of the outlet.

CH_4 oxidation was also tested but the thermal background was too high in order to get a detectable signal from the small amount of CO_2 produced. This could probably be solved by using less diluted gases to increase the amount of CO_2 produced and also by active cooling of the gas after it has passed the catalysts. This would keep the gas flow out of the tubes at a constant low temperature, such that the background level is lower and the signal to noise ratio gets higher throughout the measurement.

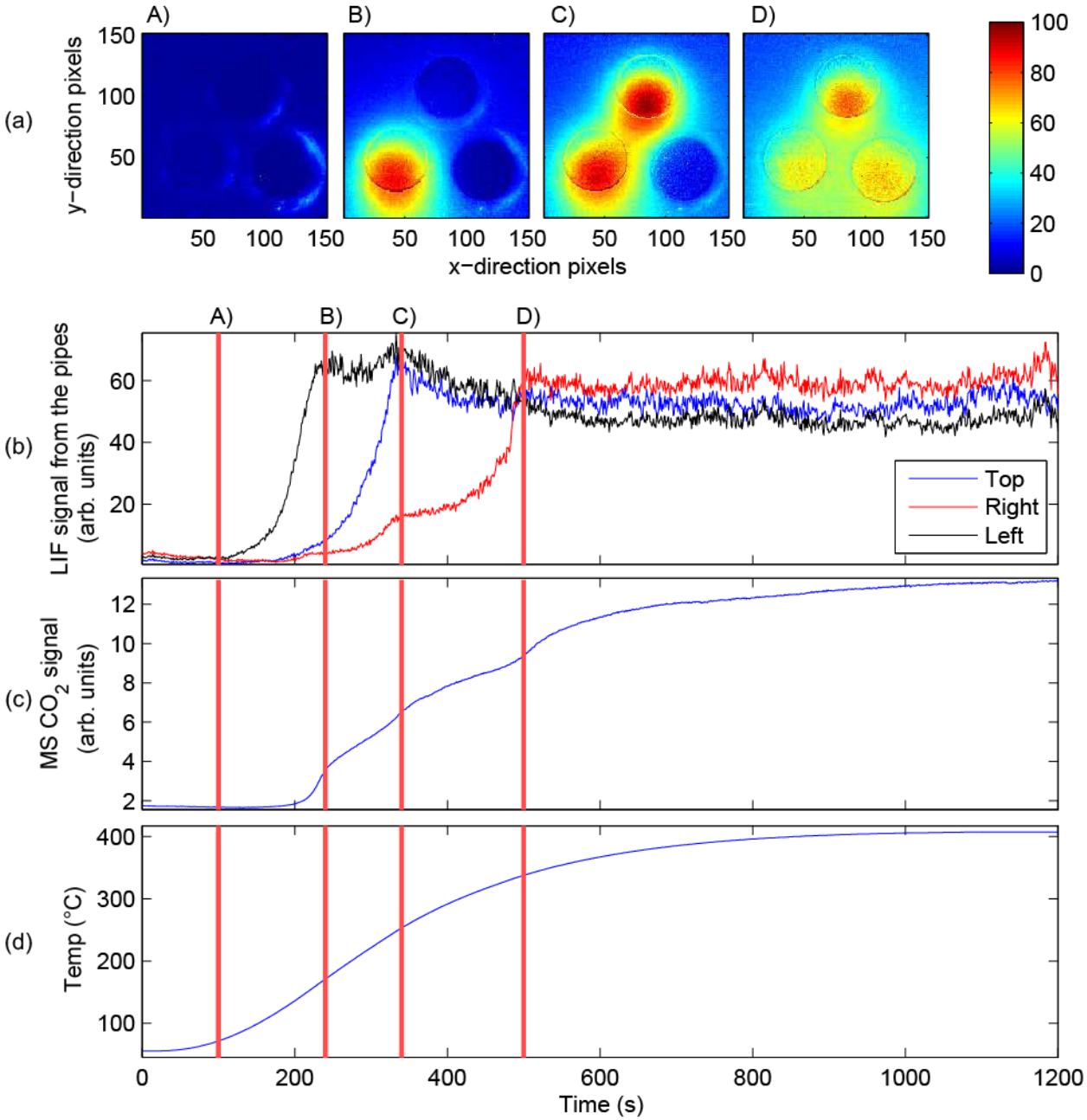

Figure 8.13. Result from an activity measurement of three catalysts simultaneously. In the smaller tubes are the samples Pt/CeO_2 (Top), Pd/CeO_2 (Left) and Pt/Al_2O_3 (right). Panel (a) shows four images A)-D) recorded by the camera at the times indicated by red lines. Panel (b) shows the average intensity inside at the tube ends, panel (c) the MS CO_2 signal and panel (d) the temperature. As the temperature is ramped up the different catalyst are activated seen both in the MS signal as an increase of the derivate and in the LIF signal as an increase at the individual tube ends. It is also seen in the images.

8.3 XRD measurements

In this section, the two reactors that were developed for combined X-ray diffraction (XRD) and mass spectrometry (MS) are described. The first reactor showed that it should be possible to perform the measurements we wanted to do, but had some severe defects. The second reactor was developed using the experience from the first and the resulting design is promising.

Included in the description of the reactors are two case studies of combined X-ray diffraction (XRD) and mass spectrometry (MS) of methane oxidation over one, but different, Pd/Al_2O_3 powder catalysts in each case. The measurements were performed at beamline i711 at MAX-lab using X-rays with a wavelength of around 1 Å.

8.3.1 Common setup

For the measurements with both reactors similar setups were used, as illustrated in figure 8.14. The reactor is either a tube or has a cavity, where the sample is placed. To the reactor is a gas system connected such that gas can be flown through the powder. The gas system is described in section 7.1. The gas is after passing the reactor analyzed by a QMS. The tube is of a material or the cavity has windows, which allows for X-rays to penetrate into the sample. The X-rays gets diffracted by the powder sample inside into different scattering angles. The diffraction pattern is recorded by a 2 dimensional flat plane detector. The beam stop avoids the detector from being destroyed by a direct hit of not diffracted high intensity X-rays.

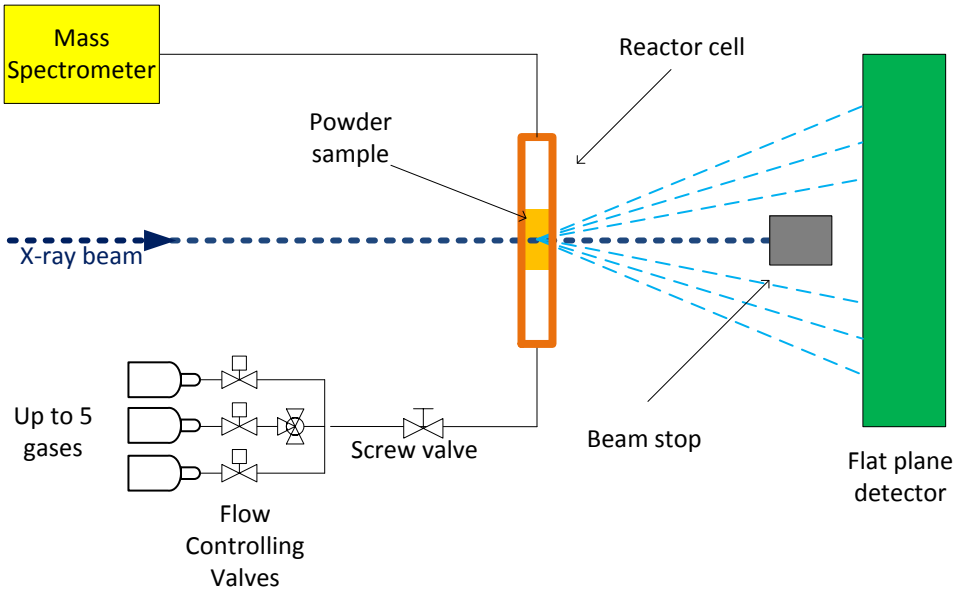

Figure 8.14. Schematic drawing of the setup.

8.3.2 The First reactor

Figure 8.15 shows an image of the first reactor. The brown/orange is an around 1 dm long and 2 mm diameter thick capton tube, which is transparent for X-rays. The powder sample is placed inside in the middle of the tube, occupying around 1 cm. At each end a quartz fiber is used to keep the sample at place. To the left of the image are the connections for the gas system.

The reactor is heated by a resistance heating wire of Kanthal coiled around the capton tube (not in the image) and the temperature is measured with a thermocouple type K outside the middle of the capton tube.

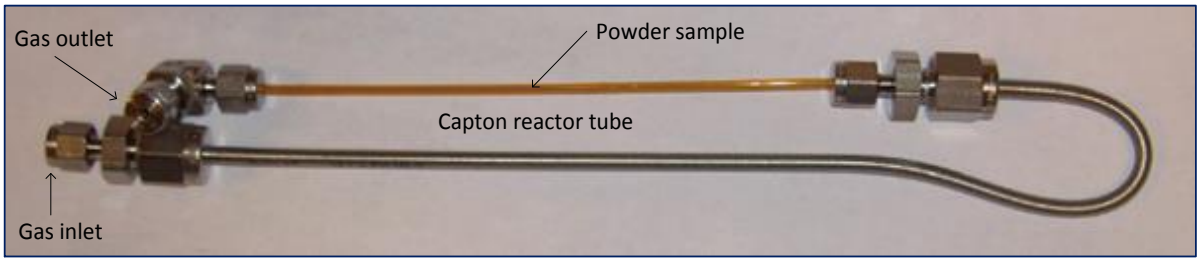

Figure 8.15. Image of the reactor. The Orange/brown is a capton tube, where the powder in the middle covering an area of roughly 1 cm. To the left are two openings for gas in- and outlet.

8.3.2.1 Reactor test

The reactor was tested with a measurement of combined XRD and MS of CH_4 oxidation over a 2% Pd/Al_2O_3 powder catalyst. The result is shown in figure 8.16. Panel (a) shows the diffractograms recorded continuously, each diffractogram recorded during 10 s. The recording started first after 1500 s. The intensity in the diffractograms is represented with the colors blue-yellow-red, in increasing order. Panel (b) shows the ratio between the sum of area A (mostly due to diffraction in PdO) and B (mostly due to diffraction in metallic Pd) of the diffractograms. Hence a higher value of the ratio indicates a higher PdO coverage.

Panel (c) and (d) shows the MS signals corresponding to the different gases in the complete methane oxidation reaction path. And panel (e) shows the temperature measured at the outside of the reactor where the powder is placed.

Between the lines (LA) and (LB), the catalyst is exposed to a flow of pure CO during a temperature ramp peaking at around 100°C. This should reduce the Pd particles by conversion of oxygen into CO_2, as indicated by the increase of the CO_2 MS signal.

After (LB) O_2, diluted to 5 % in Ar, is introduced into the flow and at (LC) the CO is removed and replaced by CH_4, also diluted to 5 % in Ar. The result is a gas mixture of about 1% CH_4, 4% O_2 and 95% Ar. Before (LD) a new temperature ramp is performed peaking at 350°C, in which the sample is activated, seen as an increase of CO_2 and H_2O, and decrease of O_2 and CH_4.

Looking at the diffractograms before and after this ramp, the intensity of the peak around A (mostly PdO) increases while B (mostly metallic Pd) decreases. The change is also clear from the ratio A/B between the peaks as shown in panel (b). During the high temperatures in the ramp no intensity is measured in the diffractograms. This was because the capton tube bended downwards due to the heat, such that no diffraction occurred and the entire X-ray beam instead hit the beam stops in front of the detector.

After (LD) a new temperature ramp is performed, where the sample gets activated again. After the second ramp no changes can be seen in the diffractogram if compared to before the ramp.

The test showed that it is possible to distinguish reduced and oxidized Pd particles in the catalyst from the diffraction pattern. However, it was not possible to follow the transformation from reduced to oxidized during a temperature ramp, since the reactor at high temperatures bends such that the X-rays miss the sample. During the measurement more disadvantages of using this thin tube as a reactor was noticed. For example, the tube was very fragile, which made it difficult to both load the sample and attach the gas line without breaking it.

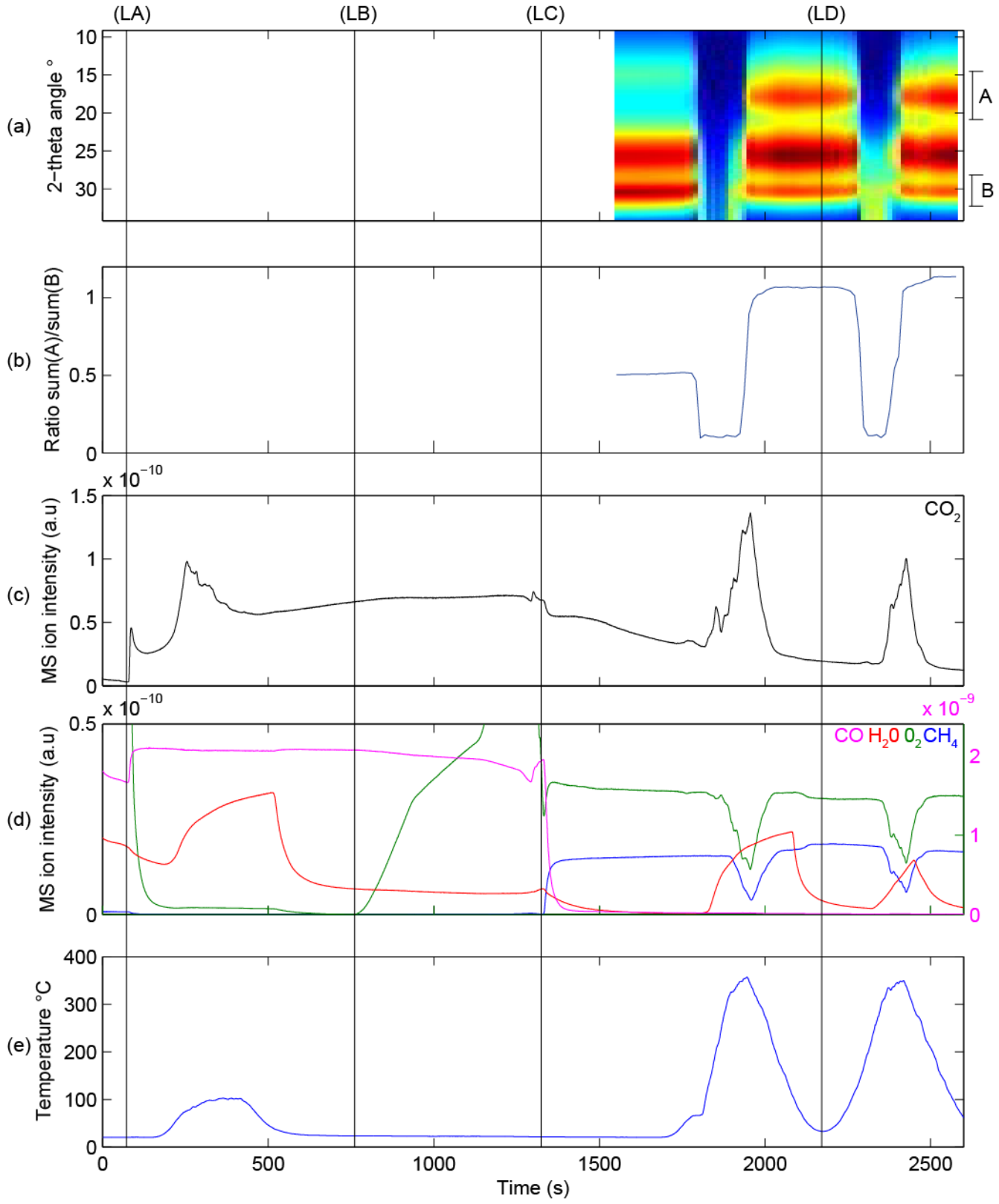

Figure 8.16. The result from the combined XRD and MS measurement of methane oxidation on a 2% Pd/Al_2O_3 powder catalyst. Panel (a) shows the diffractograms plotted with the intensity represented with the color blue-yellow-red in increasing order. Panel (b) shows the ratio between sum of A and B. Panel (c) and (d) show the MS ion intensity of the different gases in the reaction. And panel (e) shows the temperature at the outside of the middle of the reactor.

8.3.3 The Second reactor

The second reactor was developed with the experience of the first in mind and was similar to the reactor explained in [34].

Figure 8.17 illustrates the design of the second reactor for combined XRD and MS studies. The reactor consists of four different stainless steel parts, which are screwed together to one unit (e). (a) is the sample holder, (b) is the back plate, (c) is the heating plate and (d) is the front plate. The powder sample is placed in the elongated cavity in the middle of the sample holder and confined in the cavity by two carbons windows at the front and back of the holder. The carbon windows are kept in place as they are pressed against the holder by the front plate and the heating plate, as seen in figure (e). Carbon windows are transparent for X-ray, which allows for X-rays to reach the sample and get diffracted. The thickness of the powder sample the X-rays needs to penetrate in the cavity is around 3 mm. Gas pipes are connected to the small holes at the short sides of the holder such that gas can be flown through the powder in the cavity.

The sample is heated by a resistance heating wire between the heating plate and the back plate (not shown). Inside the back plate (b) is also a cavity, which can be used to cool the reactor by letting a liquid flow through. The temperature is measured with a thermocouple inserted in a hole at the top of the back plate (not shown).

This reactor is an improvement compared to the first one. The reactor is very stable and constructed of materials that can withstand high temperature. The loading of the sample is also much simpler and it is generally easier to work with, since the only fragile materials are the carbon windows, which one only needs to be in contact with when the sample should be loaded. This is a major improvement, if comparing to the capton tube that was easy to break both when loading the sample and when attaching the tube to the gas line.

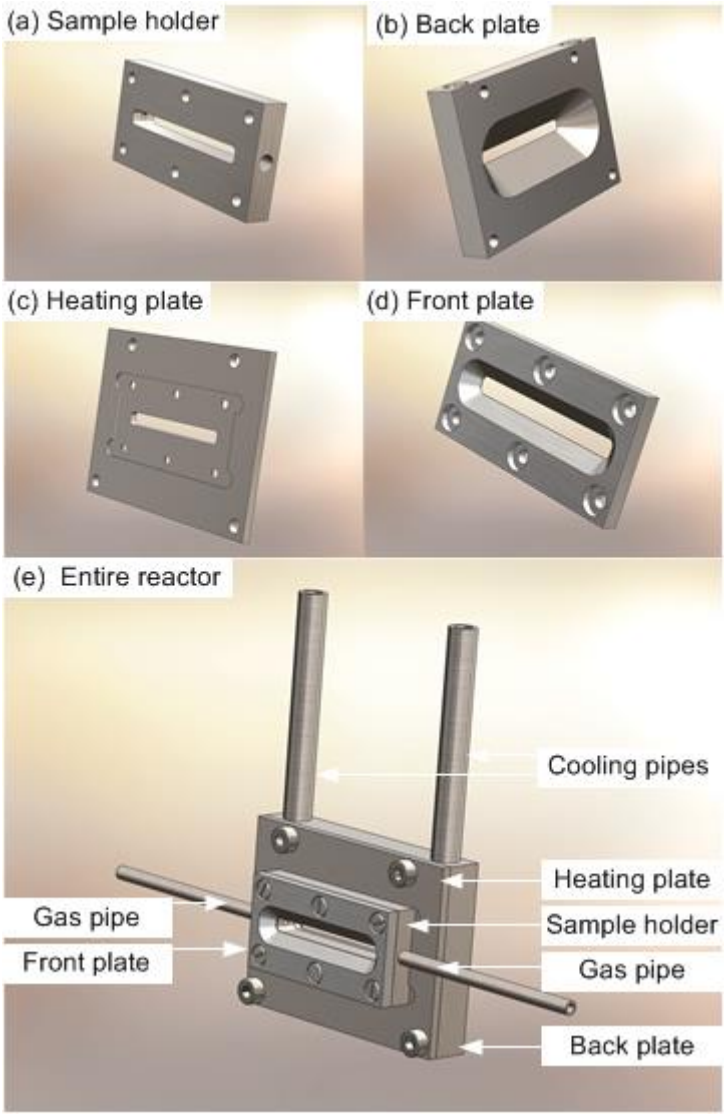

Figure 8.17. Illustration of the second reactor. It consists of four stainless steel parts (a-d) that are screwed together (e).

8.3.3.1 Reactor test

The reactor was tested with a measurement of combined XRD and MS of CH_4 oxidation over a 0.5% Pd/Al_2O_3 powder catalyst. The flow was 0.25 ml_n/min CH_4 and 0.7 ml_n/min O_2 and the pressure 1000 mbar. The O_2 and CH_4 were both diluted with 95 % Ar in the gas bottles before use. Hence, the starting condition was 13 mbar CH_4, 37 mbar O_2 and 950 mbar Ar.

During the first measurement it was seen that the thickness of the sample was problematic, since the X-rays of around 1 Å could not penetrate the sample properly. The quick solution was to fill two channels of a monolith with the sample and place the monolith in the cavity instead. This reduced the thickness of the sample to around 1 mm such that the X-ray could penetrate properly. However, this was not optimal regarding the flow through the sample, as it in the cavity between the monolith and the carbon windows will be empty space were the gas can flow more easily than through the powder in the monolith. To guide more of the gas flow through the powder, the empty space was blocked with quartz fiber.

Before the result is presented is first a general description of what is seen in the diffractograms given. Figure 8.18 (a) shows reference diffractograms for the materials that are expected to be found in the sample, i.e. Pd, PdO, Al_2O_3 and cordierite (monolith). The references are from the International Centre for Diffraction Data [35]. Each reference shows the position and the relative intensity of the peaks of that particular substance. The different references are plotted such that the highest peak in each reference is one and the other peaks relative to the highest. This is not a realistic view of the actual diffractograms of the sample consisting of only a fraction of Pd (0.5 % in the catalyst) and PdO. In reality the intensity of the Pd and PdO peaks will be much less intense than the cordierite and the Al_2O_3 peaks. This is a problem since the cordierite, which has peaks over the whole diffractogram makes it more difficult to see changes in the Pd and PdO peaks that are relatively much less intense.

Figure 8.18 (b) shows diffractograms recorded at three different temperatures during the up ramp. All peaks below 20° are found to decrease in intensity as the temperature increases. This temperature effect is general for all diffraction experiments and affects all the peaks even if it is not clear for all peaks in this measurement. The decrease of the intensity has to do with the increasing vibrations of the atoms with temperature. As the atoms vibrate they are longer time away from their periodic position in the lattice. This is seen as the amount of elastically scattered X-rays into the Bragg angle decreases, which also means that the intensity of the peaks decreases. The intensity lost is instead found as inelastic scattered X-rays in another angle than the Bragg. The inelastically scattered X-rays will be as a background over the whole diffractogram. [16]

A higher increase of the background than the decrease of peak intensity can be the reason for that the peaks above 20° in these diffractograms increase with temperature instead of decreasing. But it should not be ruled out that it may be due to structural changes of the sample. This temperature effect must be taken into account when analyzing the result. When the data is analyzed below the peaks are analyzed relatively each other.

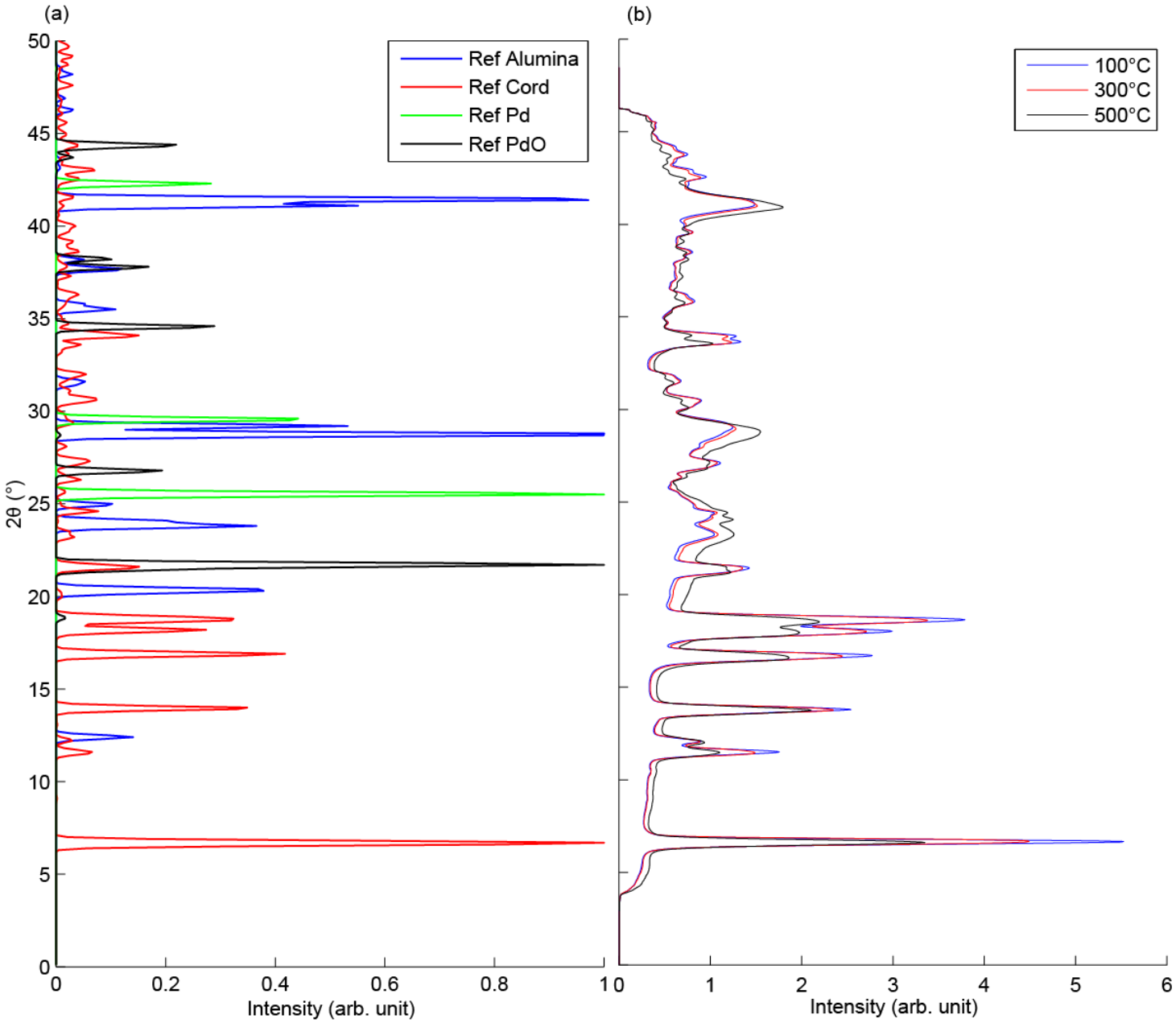

Figure 8.18. (a) shows the references for the substances in the sample, i.e. Alumina, Cordierite, Pd and PdO. (b) shows the diffractogram recorded at three different temperatures during the temperature ramp.

In figure 8.19 the results from the MS and the temperature measurements are also plotted together with the diffractograms. Panel (a) shows the diffractograms between the 2θ angles of 20° and 30°. The diffractograms are recorded continuously, each of them recorded during 10 s.

Panel (b) shows the partial pressures for the molecules that participate in either the complete or partial oxidation of methane, i.e., H_2, CH_4, H_2O, CO, O_2, Ar and CO_2. The partial pressures were calibrated according to cracking patterns and ionization probabilities, which were found in reference [36]. For example, methane was measured as mass 15 and has the cracking pattern 16/100, 15/85 14/16, 13/8, 1/4 (mass number/percent of major peak). The signal needs to be compensated for the amount of CH_4 "lost" into other mass to charge ratios. Hence, the signal was divided by the factor 85/(100+85+16+8+4). Secondly, the value was divided with the relative ionization probability, which for CH_4 is 1.6. Finally, the signals were converted to pressure. The reactants O_2 and CH_4 were scaled to the correct starting condition, 37 and 13 mbar, respectively. The products CO_2 and CO were scaled such that the sum of their partial pressures matches the drop in CH_4 partial pressure at the highest temperature. The products H_2O and H_2 were scaled in a similar way. The CO, measured as mass 28, is special as this signal also includes some of the CO_2. This was also taken into account by subtracting that amount of CO_2 from the CO signal.

Panel (c) shows the carbon (C), oxygen (O) and hydrogen (H) balances. The O balance is defined as the sum of the partial pressures of molecules including oxygen, multiplied with the number of O atoms in each molecule, normalized such that the balance is 1 if all atoms pass the reactor. For example, O_2 and CO_2 have two O atoms each while CO and H_2O has one O atom. Hence the number of O atoms corresponds to $2\times P_{O2} + 2\times P_{CO2} + 1\times P_{CO} + 1\times P_{H2O}$. This is normalized by division of the corresponding value at the beginning of the measurement. A lower value indicates that some atoms are absorbed by the catalyst, while a higher value indicates that atoms are released. Panel (d) shows the temperature, which is ramped up from 100°C to 500°C.

During the first 500 s of the temperature ramp, the H_2 pressure drops and H_2O increases, which indicates that H_2 is oxidized. This could either mean that there is some H_2 stored, and released continuously from somewhere in the system, or that H_2 is accidently flown through the reactor, e.g. through a leaking mass flow controller. Oddly, the O_2 signal does not drop in a corresponding way as the H_2 signal changes to H_2O.

As the temperature is increased further, the expected CH_4 oxidation processes takes place, where the complete oxidation is more favored than the partial as more H_2O and CO_2 is formed than H_2 and CO.

If looking how the PdO and the cordierite (cord in the plot) peak at around 21-22° changes during the up ramp, it is seen that the intensity goes down, due to the temperature effect, but also that the the PdO peak decreases more than the cordierite. Hence, this indicates that the amount of PdO decreases. If the amount of PdO decreases, the amount of Pd should increase correspondingly. This is also seen at around 26°, where there is a weak Pd peak that increases as the PdO peak goes down.

The transition from more PdO to more Pd is, however, very smooth, which makes it difficult to couple any structural change to changes in the catalytic activity. Also in the MS signal,

there are no sharp features during the temperature increase, except for when the ramp stops.

During the down ramp something strange happens with the H_2O signal. It is constant until it drops quickly at around 400°C (4000 s). As the CH_4 and O_2 do not follow this behavior, the H_2O must be formed in another way. From the mass balances, it can be seen that the amount of H and O increases during the time when the H_2O signal is constant. This can be interpreted as if stored H_2O or H and O, which react to H_2O, are released during this time. But this also means that H and O must have been stored during some other time of the ramp. It is clearly seen that H is stored (H < 1) at lower temperature during both the up ramp and especially during the down ramp. The same cannot be said about O. Another indication of storage can be that lattice constant increases as an atom is stored in the crystal. If looking at the diffractogram at the alumina peak at 29°, it is seen that peak intensity increases with temperature, probably due to an increase of the background, but it also is shifted towards lower scattering angles. Shift towards lower angle indicates that the lattice constant increases (according to Bragg's Law).

It should also be mentioned that the QMS used during the measurements gave strange signals for all masses at the time when the H_2O signal dropped quickly. The drop was seen in all the signals, but after they have been calibrated using the argon signal, assumed to be constant, the signals got the shape as they have in the figure 8.19. The drop in the H_2O signal does also have data points continuously during the drop, which is different from ordinary errors due the QMS, where a sudden drop or jump can be seen between two consecutive data points. Presently, this strange behavior of the H_2O signal has not been explained.

Aside from the problems during the test, the measurement shows that the reactor design is promising. If the problems with the too thick sample are solved without using a monolith, it should be possible to perform many catalytic measurements yielding better results. A solution would be to reduce the thickness of the sample holder part and in that way get a thinner sample.

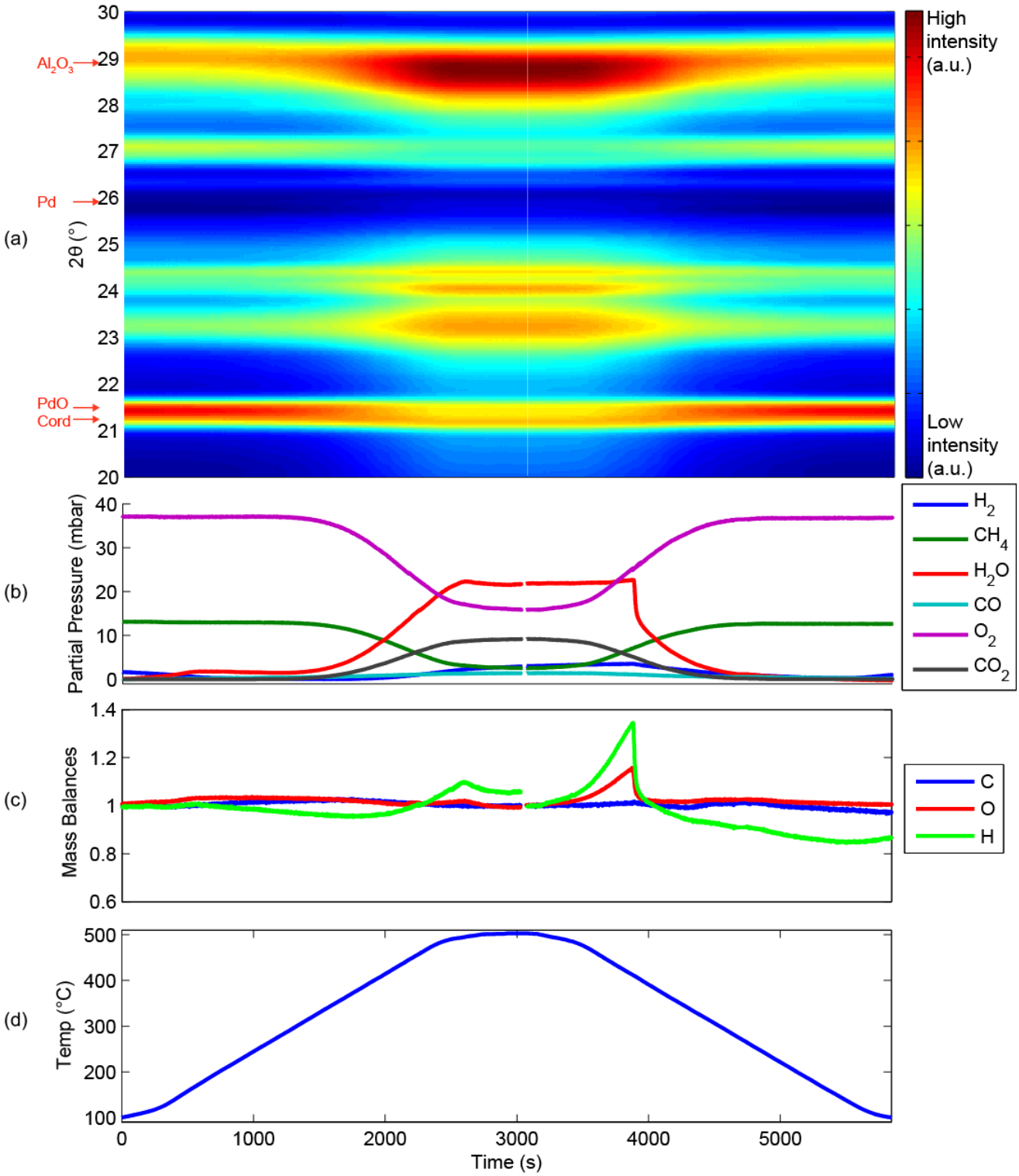

Figure 8.19. Result from the methane oxidation test over a 0.5% Pd/Al_2O_3 powder catalyst using the second reactor. (a) shows the diffractograms, (b) the partial pressures, (c) the mass balances and (d) the temperature.

9 Conclusion

In this project four different reactors were developed and tested using different case studies.

With the first reactor it is possible to measure the activity of a catalyst with mass spectrometry. Test experiments show that it is possible to measure the activity over a catalyst for temperatures up to at least 1000°C. In the cases of methane oxidation over Pd foils several interesting results were seen. For example was it possible to see how the activity of the foil depended on the history of the foil. Especially, the oxidation of methane in an oxygen rich gas flow was much more efficient after experiments under methane rich conditions. Most likely a carbide was formed in the methane rich flow, which increases the surface area and hence the catalytic conversion. The experiments in methane rich flows also show that methane is still fully oxidized to CO_2 and H_2O at low temperatures, where the Pd is expected to be oxidized, while higher temperatures promote the partial oxidation to CO and H_2. Finally, a comparison between Pd and PdAg foils show that the activity is lower over the PdAg foil than over the pure Pd foil.

With the second reactor it is possible to follow the activation of three catalysts simultaneously using planar laser induced fluorescence (PLIF). This was tested for CO oxidation over three monolith catalysts, which agreed well with previous studies [33]. However, it was not possible to measure the activity during methane oxidation, due to the high temperature needed to run this reaction, which gives a lot of thermal background. A solution to this problem would be to actively cool the gas before it is measured with PLIF.

The third and fourth reactors developed allow for structural studies of powder catalysts during catalytic reaction. The two reactors were tested with case studies of methane oxidation over Pd powder catalysts, where it was possible to see when the Pd particles were oxidized or reduced in both of the measurements. In the third setup a thin capton tube was used as a reactor. This tube was, however, difficult to work with as it was very fragile. In addition, the capton tube did not manage the high temperature needed for running the methane oxidation reaction.

The fourth reactor, which consisted of several stainless steel parts, shows promising results. It was, in comparison to the capton tube reactor, much easier to work with, although there was a problem for the X-ray to penetrate through the sample during the measurements. The solution to use a monolith to reduce the sample thickness was not a good solution, since the monolith had diffraction peaks over a broad range of angles. These peaks were also more intense than those from Pd and PdO, which made it very difficult to determine how the Pd particles changed during the measurement. But this reactor must anyway be seen as promising and if the problem with the sample thickness is solved, it should be possible to study many catalytic reactions in different harsh conditions. The case studies using the reactor did also show an interesting result. The water signal did not behave according to the expected methane oxidation reaction path, which will be interesting to study further in the future.

10 Outlook

The tests of the reactors were promising. Only minor changes are needed before they can be used for more accurate measurements. Probably many good results can be achieved from measurements with these or similar reactors in the future.

In these reactors a combination of mass spectrometry and diffraction methods were used to follow the catalytic processes. This allows for structural studies as they happen and gas composition measurements after the gas has passed the reactor. Maybe it is possible in future reactors to include planar laser induced fluorescence for studies of the gas composition close to the catalyst. This would make it possible to study how local changes in the gas composition change the properties of the catalysts.

In a couple of years the new synchrotron light source in Lund, MAX IV, is ready for use. This will push the limit of how complex systems that can possibly be studied. The X-ray will be more intense and have shorter wavelength than the X-rays used in this project, which for the diffraction measurement means that thicker samples can be studied with better time resolution, which is a clear improvement.

Catalysis is, as mentioned in the introduction involved in the manufacturing of up to 90% of all chemicals and is also used to clean toxic gases from exhaust. As many parts of the world are on the way of being industrialized, the need of chemicals and cleaning systems will increase. As the catalysts today usually consist of expensive materials, there is also a need to find cheaper materials that can be used as catalysts, but also new catalysts that can run reaction that before have not been possible to catalyze.

To find these new catalysts, a fundamental understanding of catalysis on the atomic level is of major importance.

11 Acknowledgements

First of all, I would like to thank my supervisor, Johan Gustafson, for all your help, guidance and support during the project. I am very grateful for everything I have learned and it was a very nice experience to do the project with you as my supervisor. I would also like to thank Sara Blomberg and Johan Zetterberg for all your help.

Everyone at KCK, Chalmers that have been involved in the project, thanks for your contribution. Special thanks to, Per-Anders Carlsson, Emma Adams and Sheedeh Fouladvand.

Finally, I would like to thank all of you at SLJUS division and special thanks to, Florian Bertram, Lindsay Richard Merte, Chu Zhang, Natalia Martin and Edvin Lundgren for all your help during the project.

12 References

[1] J. Berzelius, *Jahres-Bericht über die Fortscritte der Physichen Weissenschaften*, (Verlag der Laupp'schen Buchhandlung, Tübingen 1841)

[2] I. Chorkendorff and J.W. Niemantsverdriet, *Concepts of modern catalysis and kinetics,* (Wiley-VCH, Weinheim, 2nd ed, 2007)

[3] G. Ertl, *Handbook of heterogeneous catalysis,* (Wiley-VCH, Weinheim, 2nd ed ,2008)

[4] M. A. K. Khalil, *NON-CO2 GREENHOUSE GASES IN THE ATMOSPHERE,* Annu. Rev. Energy Environ. 24, (1999), 645

[5] F. Fischer, H. Tropsch, *Direct synthesis of petroleum hydrocarbons at ordinary pressure. I, II*, H. Ber. Dtsch. Chem. Ges. 59, (1926), 830

[6] M. Bowker, *The Basis and Applications of Heterogeneous Catalysis*, (Oxford University Press, USA, 1998)

[7] P. W. Atkins, *Physical Chemistry*, (Oxford University Press, Oxford, 6 ed. 1998)

[8] J. Gustafson, R. Westerström, A. Resta, A. Mikkelsen, J.N. Andersen, O. Balmes, X. Torrelles, M. Schmid, P. Varga, B. Hammer, G. Kresse, C.J. Baddeley, E. Lundgren, *Structure and catalytic reactivity of Rh oxides,* Catalysis Today 145, (2009), 227

[9] J. Gustafson, R. Westerström, O. Balmes, A. Resta R. van Rijn, X. Torrelles,C. T. Herbschleb, J. W. M. Frenken, E. Lundgren *Catalytic Activity of the Rh Surface Oxide: CO Oxidation over Rh(111) under Realistic Conditions.* , J. Phys. Chem. C. 114, (2010), 4580

[10] R. van Rijn, O. Balmes, A. Resta, D. Wermeille, R. Westerström, J. Gustafson, R. Felici, E. Lundgren, J.W.M. Frenken , *Surface structure and reactivity of Pd(100) during CO oxidation near ambient pressures*, Phys. Chem. Chem. Phys. 13, (2011), 13167

[11] A. Hellman, A. Resta, N. M. Martin, J. Gustafson, A. Trinchero, P.-A. Carlsson, O. Balmes, R. Felici, R. van Rijn, J.W.M. Frenken, J. N. Andersen, E. Lundgren, and H. Grönbeck, *The Active Phase of Palladium during Methane Oxidation*, J. Phys. Chem. Lett. 3, (2012), 678

[12] A.K. Datye, N.J. Long, *Imaging shape and structure of small metal crystallites*, Ultramicroscopy 25, (1988), 203

[13] From reference 21 in [11] "The assumption that dissociation of the first H atom is the RDS is consistent with experiments on supported catalysts, which show that the reaction order is one with respect to CH4 pressure. Previous DFT calculations indicate that the initial dissociation has the highest activation energy in the complete transformation of CH4 to elemental C and H on Pd(100) [37]. By use of a micro kinetic model, in which two different RDSs are explored (CH4 dissociation or water formation) CH4 dissociation is shown to be the RDS at all relevant reaction conditions."

[14] P. Salomonsson, S. Johansson, B. Kasemo, *Methane oxidation over PdOx: on the mechanism for the hysteresis in activity and oxygen content*, B. Catal. Lett. 33, (1994), 1.

[15] H. Gabasch,K. Hayek,B. Klötzer,W. Unterberger,E. Kleimenov,D. Teschner, S. Zafeiratos, M. Hävecker, A. Knop-Gericke, R. Schlögl, B. Aszalos-Kiss, D. Zemlyanov, *Methane oxidation on Pd(111): In situ XPS identification of active phase,* J. Phys. Chem. C, 111, (2007), 7957

[16] C. Kittel, *Introduction to Solid State Physic*. (John Wiley & Sons, New York, 1995)

[17] V. K. Pecharsky, P. Y. Zavalij, *Fundamentals of powder diffraction and structural characterization of materials*, (Springer; 2nd ed. 2009)

[18] http://www.esrf.eu/computing/scientific/FIT2D/

[19] http://www.pfeiffer-vacuum.com

[20] P. E. Miller, M. B. Denton. *The quadrupole mass fillter: Basic operation concepts.* J. Chem. Educ. 63, (1986), 617
[21] http://www.qmg700.com/quadinfo/Literature/Quadrupole
[22] W. Kang, O. Fujita and K. Ito, *Visualization of formaldehyde distribution above platinum plate catalyst by using LIF method,* J. Energ. Resour-Asme. 118, (1996), 82
[23] F. Gudmundson, J. L. Persson, M. Forsth, F. Behrendt *B. Kasemo, A. Rosén*, *OH gas phase chemistry outside a Pt catalyst,* J. Catal. 179, (1998), 420
[24] J. Zetterberg, S. Blomberg, J. Gustafson, Z. W. Sun, Z. S. Li, E. Lundgren and M. Aldén, *An in situ set up for the detection of CO2 from catalytic CO oxidation by using planar laser-induced fluorescence,* Rev. Sci. Instrum. 83, (2012), 053104
[25] S. Svanberg, *Atomic and Molecular Spectroscopy Basic Aspects and Molecular Spectroscopy,* (Springer; 4th edition, 2004)
[26] http://www.bronkhorst.com/
[27] http://www.swagelok.com/
[28] http://www.kanthal.com/
[29] http://www.goodfellow.com/
[30] M. Batzill, *The surface science of graphene: Metal interfaces, CVD synthesis, nanoribbons, chemical modifications, and defects",* Surface Science Reports, 67, (2012) 83
[31] A.Resta, J. Gustafson et al. unpublished
[32] G. Attard, C. Barnes, *Surfaces,* (Oxford University Press, Oxford 1998)
[33] Yu Yao, Y. F. *The Oxidation of CO and Hydrocarbons over Noble Metal Catalysts*. J. Catal., 87, (1984), 152.
[34] S. Hannemann, M. Casapu, J.-D. Grunwaldt, P. Haider, P. Trüssel, A. Baikera ,E. Welterbet, *A versatile in situ spectroscopic cell for fluorescence/transmission EXAFS and X-ray diffraction of heterogeneous catalysts in gas and liquid phase,* J. Synchrotron Rad. 14, (2007), 345
[35] The International Centre for Diffraction Data, http://www.icdd.com/
[36] RGA Application Bulletin #208 Spectra Reference, http://www.mksinst.com/docs/R/SpectraBulletin208.pdf
[37] C. J. Zhang, P. Hu, Methane Transformation to Carbon and Hydrogen on Pd(100): Pathways and Energics from Density Functional Theory Calculations, J. Chem. Phys. 116, (2002), 322
[38] W. Demtröder, *Laser Spectroscopy Basic Concepts and Instrumentation*, (Springer; 3rd edition, 2003)